Receiver functions in the western United States, with implications for upper mantle structure and dynamics

Hersh J. Gilbert,[1] Anne F. Sheehan, Kenneth G. Dueker,[2] and Peter Molnar

Cooperative Institute for Research in Environmental Sciences and Department of Geological Sciences, University of Colorado, Boulder, Colorado, USA

[1]   Investigations into mechanisms driving surface tectonics commonly search for mantle sources, but few observations constrain flow in the upper mantle and transition zone. Here variations in the upper mantle discontinuities at 410 km and 660 km below the western United States are revealed through mapping depths of compressional-to-shear wave conversions recorded by broadband seismometers. The resulting image exhibits 20 and 30 km of topography on the 410- and 660-km discontinuities, similar depth variations to those seen where subducting slabs of lithosphere reach the transition zone. The pattern of discontinuity topography imaged here does not correlate with the surface tectonics of the Rocky Mountains, Colorado Plateau, or Basin and Range Province, providing no support for upward and downward flow at transition zone depths controlling surface topography and deformation in this region, at least at scale lengths of a few hundred kilometers. Furthermore, we find no clear correlation between the depths of the 410- and 660-km discontinuities. Undulations on the surfaces of both discontinuities appear to be spaced at distances of ~800 km. If the topography were due only to lateral temperature differences, such differences would be comparable to those where slabs sink and might suggest separate convective flow above and below the transition zone. Alternatively, the topography may reflect lateral variations in composition. Variations in the sharpness of converted phases across the region offer some support for compositional heterogeneity, but the lack of a correlation between sharpness and depth casts doubt on this explanation for the variations in depth.   *INDEX TERMS:* 7203 Seismology: Body wave propagation; 7207 Seismology: Core and mantle; 7218 Seismology: Lithosphere and upper mantle; 8121 Tectonophysics: Dynamics, convection currents and mantle plumes; 8124 Tectonophysics: Earth's interior—composition and state (1212); *KEYWORDS:* upper mantle discontinuities, mantle convection, western United States tectonics, mantle composition, phase transitions

1. Introduction

[2]   During the Cenozoic era a combination of subduction of the Farallon plate and extension of the Basin and Range Province has produced a region with complex upper mantle composition and thermal structure beneath the Colorado Plateau, Basin and Range Province, and Rocky Mountains. Studies have found highly heterogeneous seismic wave speeds in the upper 300-km of this region [*Humphreys and Dueker*, 1994] within a background of low speeds compared with the global average [*Alsina et al.*, 1996]. In contrast, regions of high speed prevail at greater depths in the mantle transition zone [*Bijwaard et al.*, 1998; *van der Lee and Nolet*, 1997]. *Eaton* [1986] attributed high elevations in this region to thermal expansion of unusually hot material within the uppermost mantle beginning in the Miocene and culminating as recently as 4–7 Ma. The presence of warm material rising vertically from transition zone depths or deeper would imply a thin mantle transition zone beneath the region. *Bird* [1979] however, attributed the high Colorado Plateau and Laramide uplifts to basal tractions associated with the flat Farallon slab removing the upper mantle portion of the lithosphere by delamination, thereby causing the remaining lithosphere to rise. In contrast to uplift mechanisms associated with warm buoyant material rising from great depths, this mechanism would result in the removal of cool material, which might be detectable in the transition zone, and its replacement by hotter material from the asthenosphere. As numerous studies of dynamic topography have shown [e.g., *McKenzie*, 1977; *Parsons and Daly*, 1983; *Richards and Hager*, 1984], when not dominated by other processes, positive regional topography correlates with the direction of convective flow beneath the

---

[1]Now at Department of Geosciences, University of Arizona, Tucson, Arizona, USA.

[2]Now at Department of Geology and Geophysics, University of Wyoming, Laramie, Wyoming, USA.
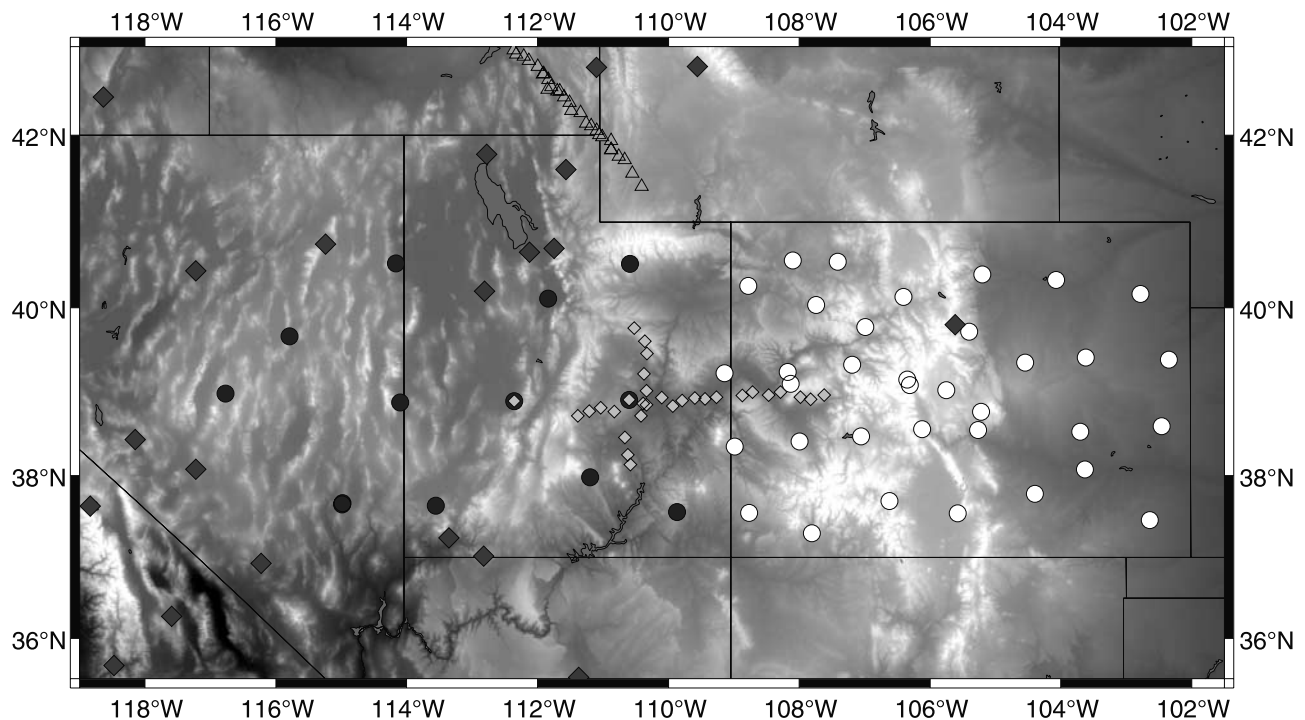
Figure 1. Map of seismic stations comprising arrays in the western United States used in this study. Each different Program for Array Seismic Studies of the Continental Lithosphere (PASSCAL) experiment and USNSN stations are coded by different symbols. RMF stations, open circle; CPGB, solid circles; DPU, open diamonds; SRP, triangles; and USNSN, solid diamonds.

surface. Thus it makes sense to look in the underlying mantle for heterogeneity that correlates with processes occurring at the Earth's surface.

[3] Phase transitions of the mantle minerals olivine to wadsleyite and ringwoodite to perovskite + magnesiowustite are thought to cause major seismic discontinuities at the nominal depths of 410 and 660 km in the Earth's mantle. Numerous studies have used the Clapeyron slopes for these transitions (3.0 MPa/K for the 410-km discontinuity and −2.0 MPa/K for the 660-km discontinuity [*Bina and Helffrich*, 1994]) and the depth of the discontinuities to infer lateral temperature variations in the upper mantle [e.g., *Dueker and Sheehan*, 1998; *Li et al.*, 1998; *Shen et al.*, 1998b; *Collier and Helffrich*, 2001; *Lebedev et al.*, 2002]. The magnitude of the Clapeyron slopes for these two phase transitions predict that the depth of the 410-km discontinuity would be displaced 50% more than that of the 660-km discontinuity and in the opposite sense by the same thermal anomaly. However, more topography is usually found on the 660-km discontinuity than on the 410-km discontinuity [e.g., *Flanagan and Shearer*, 1998; *Li et al.*, 1998], indicating either that thermal perturbations at the two discontinuities differ or that a factor other than temperature regulates discontinuity depths. Mineralogical investigations have shown that variations in the iron [*Irifune and Isshiki*, 1998] and aluminum [*Weidner and Wang*, 1998] content in the mantle, as well as the presence of hydrogen [*Yusa and Inoue*, 1997; *Yusa et al.*, 2000], can affect the depth, impedance contrast, and sharpness of these seismic discontinuities. Additionally, the discovery of a greater impedance contrast associated

with the 410-km discontinuity beneath oceanic regions than continental shields [*Gu et al.*, 1998] has stimulated arguments for regional variations in mantle olivine content [*Agee*, 1998].

[4] The upper mantle beneath a large region of the western United States can be studied by combining data from several arrays of portable and permanent broadband seismometers. Utilizing data from multiple data sets increases the spatial extent over what previous studies have imaged. Important characteristics of mantle structure, which cannot be detected with smaller arrays, become apparent in a larger-scale study. One such characteristic is the horizontal scale of variations in discontinuity structure; by studying the discontinuities over a large enough area, we can examine whether or not characteristic wavelengths dominate discontinuity topography.

2. Data and Processing

[5] To investigate the upper mantle discontinuity structure below this region we analyzed data collected from a number of Program for Array Seismic Studies of the Continental Lithosphere (PASSCAL) deployments of broadband seismometers in the western United States, including the Snake River Plain (SRP) [*Dueker and Humphreys*, 1993], Rocky Mountain Front (RMF) [*Sheehan et al.*, 1995], Colorado Plateau-Great Basin (CPGB) [*Sheehan et al.*, 1997], and Green River (DPU) [*Bump et al.*, 1995] experiments (Figure 1). Data from permanent seismic stations from the U.S. National Seismic Network (USNSN) have supplemented portable station data.

[6] Here, we report observations of P-to-S wave conversions from the 410- and 660-km discontinuities ($P_{410}s$ and $P_{660}s$, where $P_d s$ denotes a P-to-S conversion at depth d) beneath a large portion of the western United States. We calculated teleseismic receiver functions [*Langston*, 1977] that isolate energy produced by P-to-S wave conversions at discontinuities in seismic wave speeds.

[7] Receiver function calculation entails deconvolving the vertical from radial components of ground motion to produce a seismic time series that reflects characteristics of the impedance contrasts below the receiver. We visually inspected the raw seismic traces to avoid noisy traces. We then processed receiver functions and removed those with overly energetic codas using a cutoff based on levels of root mean square amplitudes. This left nearly 1000 radial receiver functions. We initially used the one-dimensional tectonic North America (TNA) velocity model [*Grand and Helmberger*, 1984] and a V_p/V_s ratio of 1.84 [*Dueker and Sheehan*, 1998] for mapping $P_d s$ arrival times to depths. Time corrections for lateral variations in seismic wave speeds were found by first calculating ray paths using the one-dimensional TNA velocity model [*Grand and Helmberger*, 1984], and then summing travel time residuals along these paths through a regional three-dimensional P wave model [*Dueker et al.*, 2001]. P wave residuals (δt_P), ranging between ±1 s, were rescaled to S wave residuals (δt_S) using a $\delta t_S/\delta t_P$ of 2.4 [*Dueker and Sheehan*, 1998] and adjusted to account for the difference in path length between the P and S legs. We use the tomographic model of *Dueker et al.* [2001] for three reasons. First, data collected from the same stations used in this receiver function study were used to produce the tomographic model; therefore the model has a large number of rays sampling the region of interest. Second, the model offers higher spatial resolution than other models that include this region [e.g., *Bijwaard et al.*, 1998; *van der Lee and Nolet*, 1997]. The use of a global model to calculate timing corrections that used data from fewer stations in this area would not correct for small-scale heterogeneities as effectively as this regional model does. Finally, use of a single model to correct the entire data set avoids shifts that can be introduced when combining multiple independent models. We then applied timing corrections by stretching and contracting the time to depth conversion for each receiver function and band-pass filtered each receiver function in the band of 0.03 to 0.15 Hz.

[8] To enhance the signal-to-noise ratio, we stack receiver functions. Stacking all data used in this study reveal depths of the upper mantle discontinuities below the western United States at 410 ± 1 km and 654 ± 2 km (Figure 2). Contrary to global average P and S wave velocity structures, for which the 410-km discontinuity impedance is smaller than that of the 660-km discontinuity, we found similar amplitudes for the $P_{410}s$ and $P_{660}s$ phases averaged for all the receiver functions, with a narrower $P_{410}s$ pulse. Investigating the Rocky Mountains, *Dueker and Sheehan* [1998] found the average discontinuity depths at 419 and 677 km referenced to the TNA velocity model and a larger $P_{660}s$ amplitude. The different mean depths found for the 660-km discontinuity between this study and the earlier work by *Dueker and Sheehan* [1998] results in part from our including a larger region where the discontinuities shallow. Additional discrepancies result from our correcting for
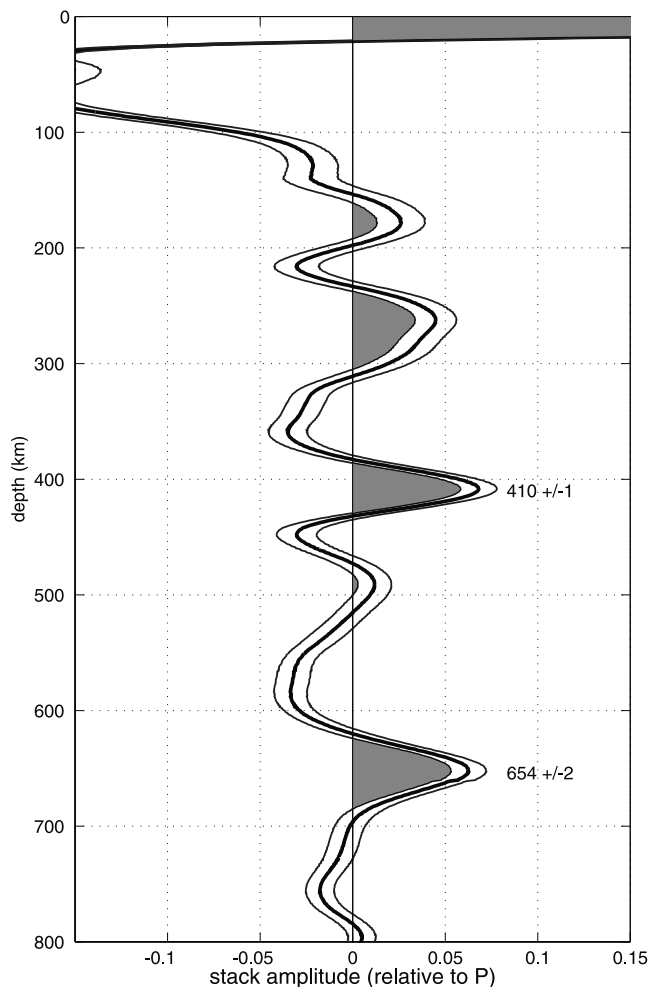

Figure 2. Stack of all moveout-corrected radial receiver functions included in this study shown as thicker line. Error bounds of the receiver function stack, found using bootstrap resampling, are shown as thinner lines.

lateral heterogeneity using residuals calculated from the P wave model of *Dueker et al.* [2001] to a depth of 700 km, while *Dueker and Sheehan* [1998] applied corrections based on the S wave model of *Lee and Grand* [1996] to a depth of 400 km. Although the absolute depths of the discontinuities depend on the velocity model chosen, here we focus on geographic variations in structure, as they are less sensitive to the velocity model.

[9] Stacked data from individual stations used in this study display variations in discontinuity depths and in the amplitudes of $P_{410}s$ and $P_{660}s$ phases both azimuthally at a single station, and between stations. For example, stations BMN (Figure 3a) and ELK (Figure 3b), both in the Basin and Range Province in northern Nevada, show arrivals for the 410-km discontinuity that vary little with azimuth, with the exception of the southeast back azimuth for station BMN. Below both of these stations, however, depths of the 660-km discontinuity vary with azimuth; those to the southeast of BMN appear to be shallow and those to the northwest appear either deeper or are recorded with much lower amplitude. At station ELK, the 660-km discontinuity appears to have similar depths to the southeast and north-
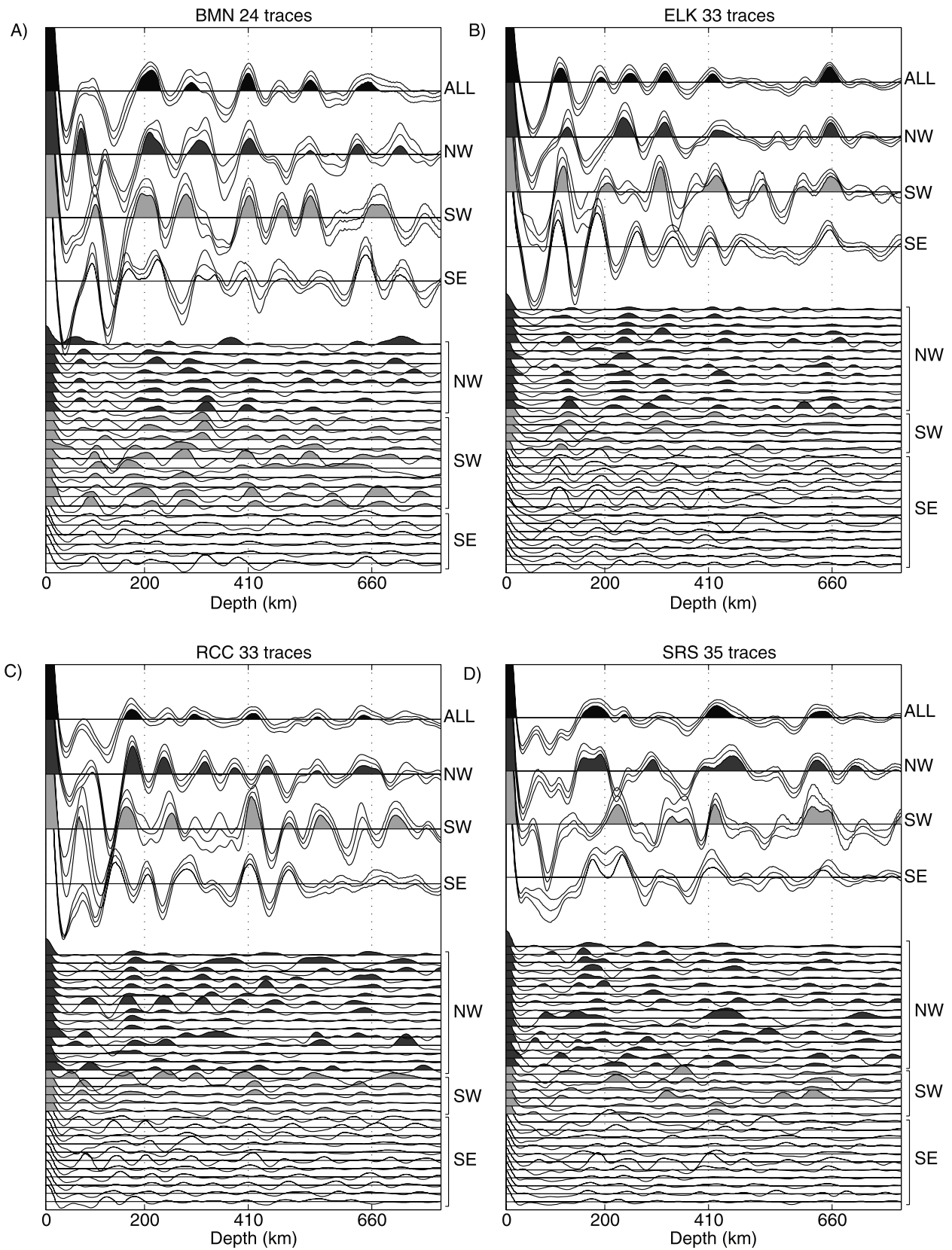
Figure 3. Receiver functions, back azimuth bin stacks, and stacks of all receiver functions recorded by four stations used in this study (a) BMN, (b) ELK, (c) RCC, and (d) SRS. Lower set of traces shows individual receiver functions ordered by back azimuth as noted by the bins to the right of the traces. Stacked traces are shown larger above and labeled for each azimuth bin SE (southeast), SW (southwest), NW (northwest), and ALL (all back azimuths). Error bounds, found by bootstrap resampling data for each azimuth bin and station, are presented for the stacked traces.

west, but the depth of the discontinuity to the southwest cannot be picked with as much confidence due to multiple peaks. Stations RCC (Figure 3c) and SRS (Figure 3d), both on the Colorado Plateau in Utah, have azimuthally variable depths for both discontinuities. Observations made from data collected at these stations illustrate how stacking all the data collected at single stations can obscure lateral variations. Smaller amounts of topography reported by studies comparing average depths below individual stations [e.g., *Chevrot et al.*, 1999; *Ramesh et al.*, 2002] may underestimate lateral variability in depths.

[10] To determine lateral variations in discontinuity structure we sorted receiver functions into common conversion point bins (CCP), which is analogous to common midpoint stacking. Thus we stack receiver functions whose ray paths cross the discontinuities at short distances from one another. Bins combining data from multiple stations improve the signal-to-noise ratio by stacking down signal-generated noise related to topographic scattering [*Clouser and Langston*, 1995]. Our receiver function stacking follows the procedures of *Dueker and Sheehan* [1998] with modifications. First, each of the receiver functions are processed and filtered in the manner described above, and we then calculate piercing points of the P_ds rays at 2 km depth intervals by tracing the ray paths using the TNA velocity model. We define a 3-D grid of sample points at 75 km by 75-km lateral spacing and at every 2-km depth interval within a 1500-km (east-west) by 800-km (north-south) by 875-km (vertical) volume (Figures 4a and 4b). For each depth interval, the P_ds rays in a 225×225 km^2 area centered on each sample point are stacked. By stacking receiver functions for every sample point at 2-km depth intervals we account for horizontal displacement of the P_ds ray path between where it samples the 410- and 660-km discontinuities, note the slight differences in sampling between Figures 4a and 4b. Using this method of stacking, some of the rays within a given column of bins at 410 km depth will not be included in same column at 660 km depth.

[11] A three-dimensional image of transition zone structure is constructed by finding discontinuity depths within each column of bins. Using bootstrap resampling [*Efron and Tibshirani*, 1986] for each bin, we randomly selected amplitudes of receiver functions and summed them to obtain 200 estimates of the mean amplitude for that bin. For each bin of n traces, all 200 resamplings used the same number n of randomly selected amplitudes and hence multiple samples of some traces. The distribution of those 200 receiver function amplitudes yields a mean amplitude and standard deviation for each bin. Then, for each column of bins, we examined the resulting distribution of receiver function amplitudes as a function of depth in the ranges of 360–460 km and 615–715 km to pick and record the maxima. To determine the depths of the discontinuities we used the median in the 60 km depth range surrounding the mode (most frequently picked depth) of each distribution (Figures 5a and 5b). We then estimated confidence limits for each column by determining the depth interval containing 66% of the picks. We excluded estimated depths with broad distributions, where 66% of the picks do not lie within 9 km of the median. The remaining depth estimates are all fit to more finely

sampled surfaces with 10-km grid spacing using the interpolation method of *Sandwell* [1987].

3. Observations

3.1. The 410- and 660-km Discontinuities

[12] The 410-km discontinuity, whose depths vary by more than 20 km across the region, is deepest below the central Colorado Plateau in Utah and the northern Basin and Range in northern Nevada and shallowest in northern Colorado and southern Wyoming below the Rockies and beneath the southern Basin and Range (Figure 6a). Depths of the 660-km discontinuity, which vary by 30 km, are deepest below northern Colorado and the northern Basin and Range in northwestern Nevada, and shallowest in the central Colorado Plateau in southern Utah and the northeastern Basin and Range in Nevada (Figure 6b). Transition zone thickness, given by differences in depths of the 410- and 660-km discontinuities, varies between 220 km and 270 km. The stack of all receiver functions (Figure 2) shows a transition zone thickness of 244 ± 9 km, close to the global average value of 241 km found by *Flanagan and Shearer* [1998] using *SS* precursors.

[13] For comparison purposes, we also present maps of the discontinuity depths made using only the one-dimensional TNA structure (Figures 7a and 7b) thus ignoring effects from lateral heterogeneities in seismic wave speeds. The application of laterally varying timing corrections sharpened the distributions of picked depths; the average standard deviations for the 410- and 660-km discontinuity depths corrected using the model of *Dueker et al.* [2001] are 5.4 km and 6.1 km, respectively, compared with 5.7 km and 7.2 km for the same columns of bins when lateral heterogeneity is ignored. Inspection of the general discontinuity structure indicates that applying timing corrections introduces only minor modifications that change where the discontinuities deepen or shallow (compare Figures 6 and 7). Additionally, we test to determine if the application of lateral heterogeneity corrections affects the scale length of the discontinuity structure. We find that the power spectra of the discontinuity surfaces for the corrected and uncorrected data set are very similar (Figures 8a and 8b). Conversely, the power spectra produced by applying corrections to a flat surface exhibit considerably smaller peaks at different wavelengths (Figure 8c). This test helps to further confirm that lateral heterogeneity corrections are not responsible for the observed scale length of discontinuity structure.

[14] Depths of the 410- and 660-km discontinuities are not correlated (Figure 9a). To further demonstrate that lateral heterogeneity corrections do not influence the correlation of the discontinuity depths, we present a correlation plot between the depths of the discontinuities found by making no corrections for lateral variations in wave speeds (Figure 9b). Examining changes in depths between the corrected and uncorrected discontinuity surfaces indicates that there is no simple relationship between the two, but that most of the depths do not differ by more than ~5 km (Figure 9c). By excluding depth estimates with large deviations from the median depth of each discontinuity we determine how well the remaining points correlate (Figures 9d and 9e). For this test we included only depth estimates for columns with
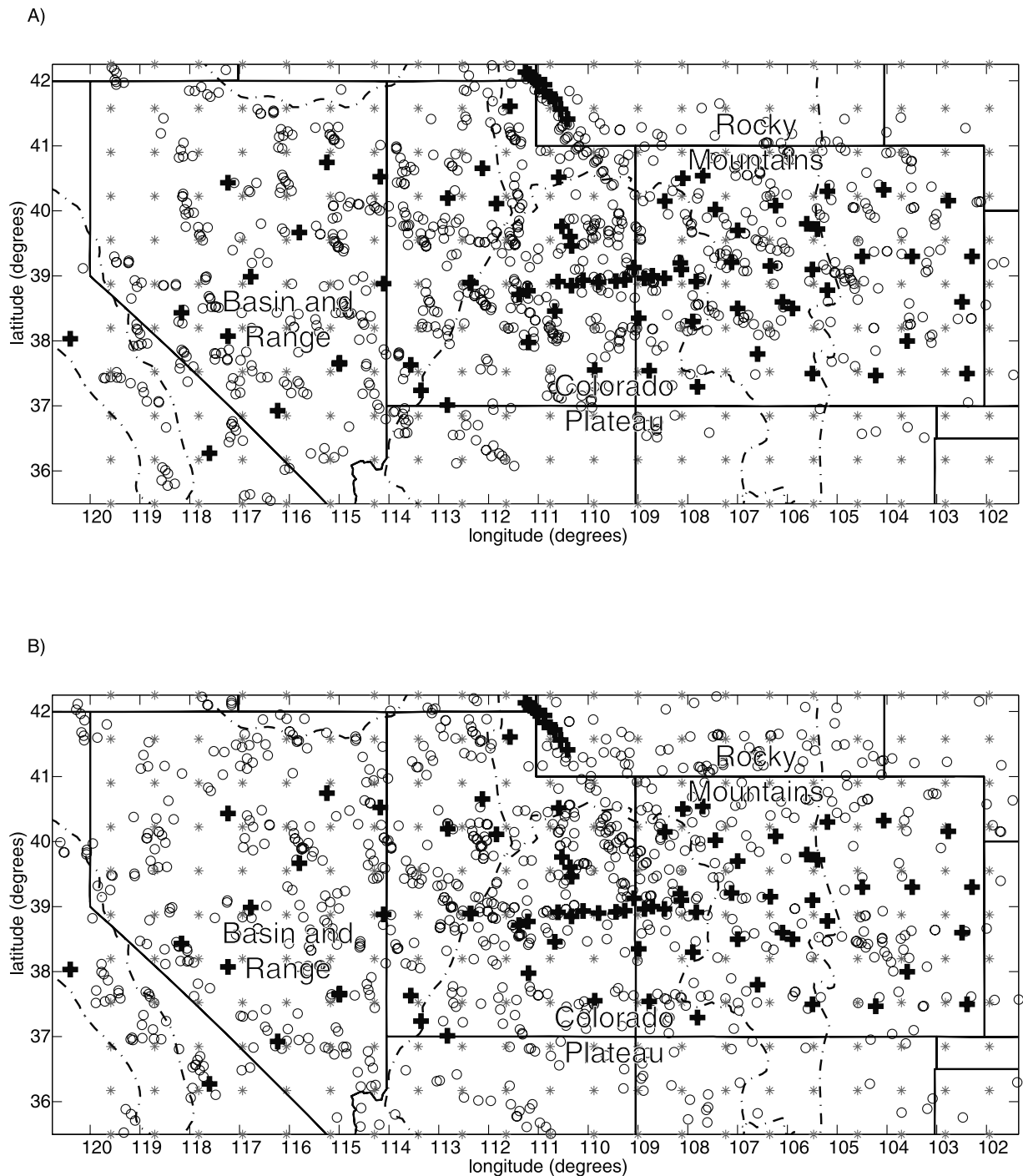
A)

B)

Figure 4. Map showing $P_d s$ wave piercing points (circles), which fan out away from each station with increasing depth. Points shown here correspond to the locations of the $P_d s$ rays at (a) 410 and (b) 660 km depths. Common conversion point bin locations are shown as asterisks spaced at 75 km. Seismic stations contributing data are shown as solid pluses. Boundaries between Rocky Mountains, Colorado Plateau, and Basin and Range are shown as dashed lines.

corrected depths between 400 and 420 km for the 410-km discontinuity and between 640 and 670 km for the 660-km discontinuity. The calculated slopes do not change greatly when fitting either the whole or reduced data sets. Figure 9f, which is the same as Figure 9c with the reduced data set, gives a clearer picture that there is no simple pattern by which the corrected depths change from the uncorrected.

[15] To further examine the existence of any possible correlation between the discontinuity depths, we calculated the two-dimensional cross correlation of the discontinuity surfaces. This test is apt to identify any possible shift that could be applied to either discontinuity that could improve the correlation between the discontinuities. Such a test is necessary to identify correlated or anticorrelated disconti-
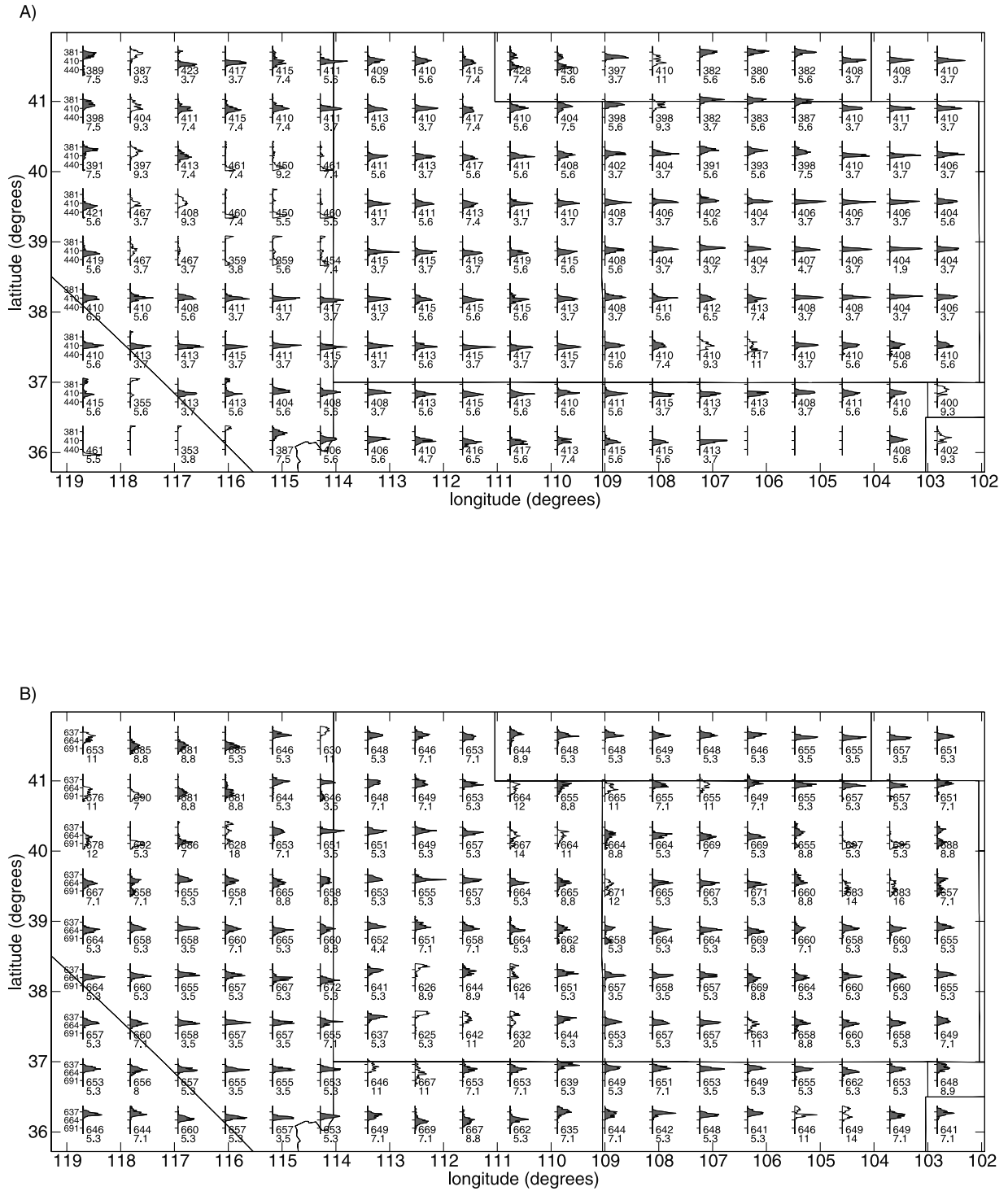
Figure 5. Histograms of discontinuity depths for the (a) 410- and (b) 660-km discontinuities. Each histogram represents the distribution of maximum amplitudes for receiver function stacks within each column of bins found for each of 200 bootstrap realizations within the depth range of 360–460 km for the 410-km discontinuity and 615–715 for the 660-km discontinuity. By finding the trimmed median of picks within 30 km of the mode of each distribution we determine the depth of the discontinuity within each bin along with its associated error. Histograms are plotted geographically at the location of their corresponding column of bins and labeled with their picked depths and associated uncertainty. Columns of bins with uncertainties over 9 km are not used in determining the discontinuity structures and are not filled in here.
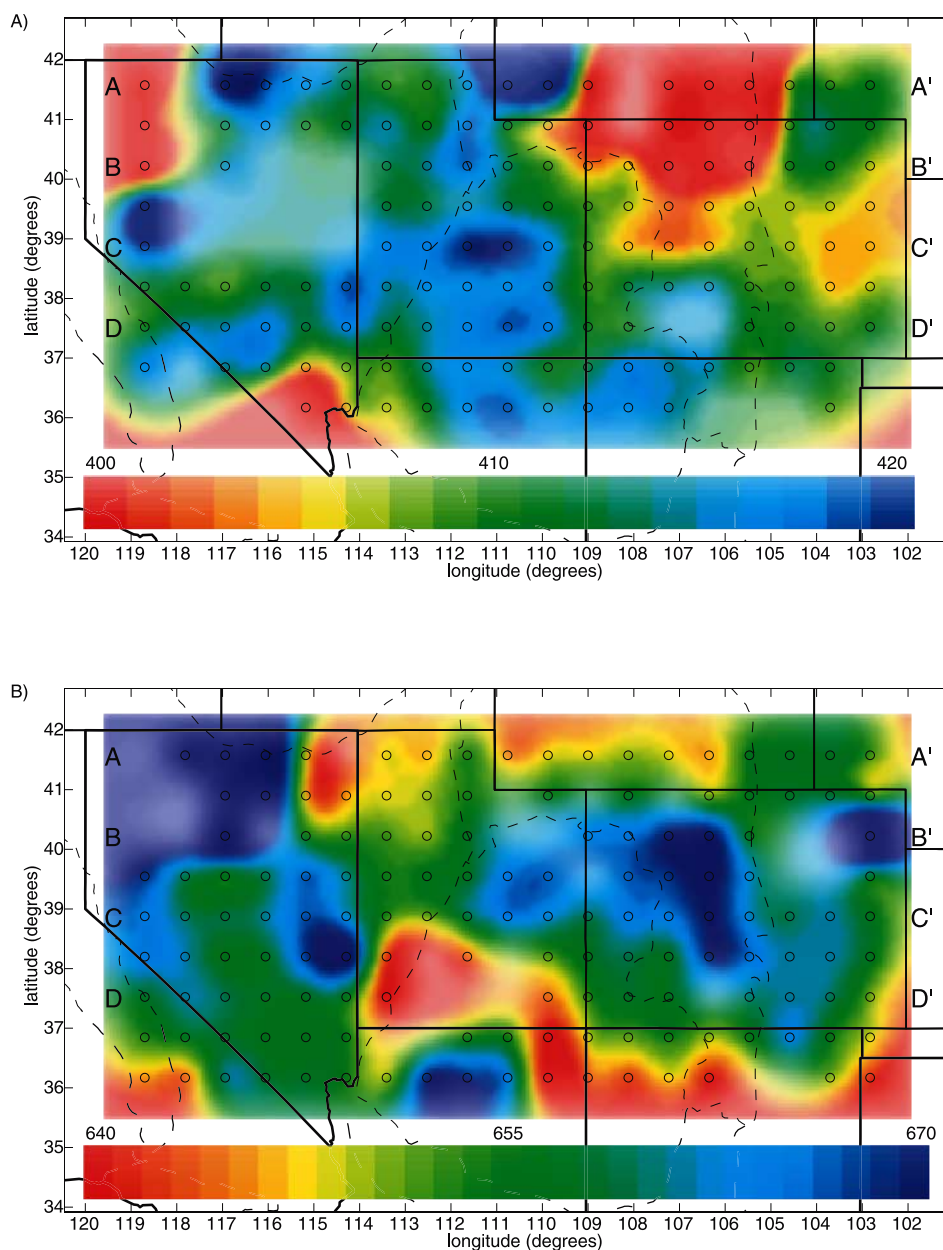
Figure 6. Map views of surface depths of the (a) 410- and (b) 660-km discontinuities. Depths greater than 410 or 660 km are shown as blue colors for each discontinuity while red colors indicate shallow depths. Color saturation for the images is scaled by the standard deviation (σ) of the depths (least saturated is >9 km uncertainty; the most saturated show $\sigma = 3$ km on the 410-km discontinuity and $\sigma = 4$ km on 660-km discontinuity). Locations of bin center points for which depth estimates are used are shown as black circles. Also shown are boundaries (dashed line) between Rocky Mountains, Colorado Plateau, and Basin and Range provinces.

nuity structure if the thermal structure of the mantle is not vertically coherent, such as in a subduction zone where the dip of the slab is not vertical, and some offset is observed between where the slab interacts with the discontinuities. Figure 10 shows that the correlation for the unshifted discontinuities is weak (correlation coefficient value of 0.1). We find a maximum positive correlation coefficient of 0.3, which is also a weak correlation, by shifting the 410-km discontinuity to the east ~500 km relative to the 660-km discontinuity, while the most negative (or most anticorrelated) coefficient of -0.3 is found when shifting the 410-km discontinuity to the west ~200 km, and to the north ~50 km. If the observed anti-correlated topography resulted from the presence of a slab, the slab would be dipping to the west, which is the opposite direction of the subducted Farallon plate. This observation further indicates that it is unlikely that the discontinuity topography results from the presence of a subducted slab.

[16] To help assess whether the observed discontinuity topography is some sort of artifact, we created randomized
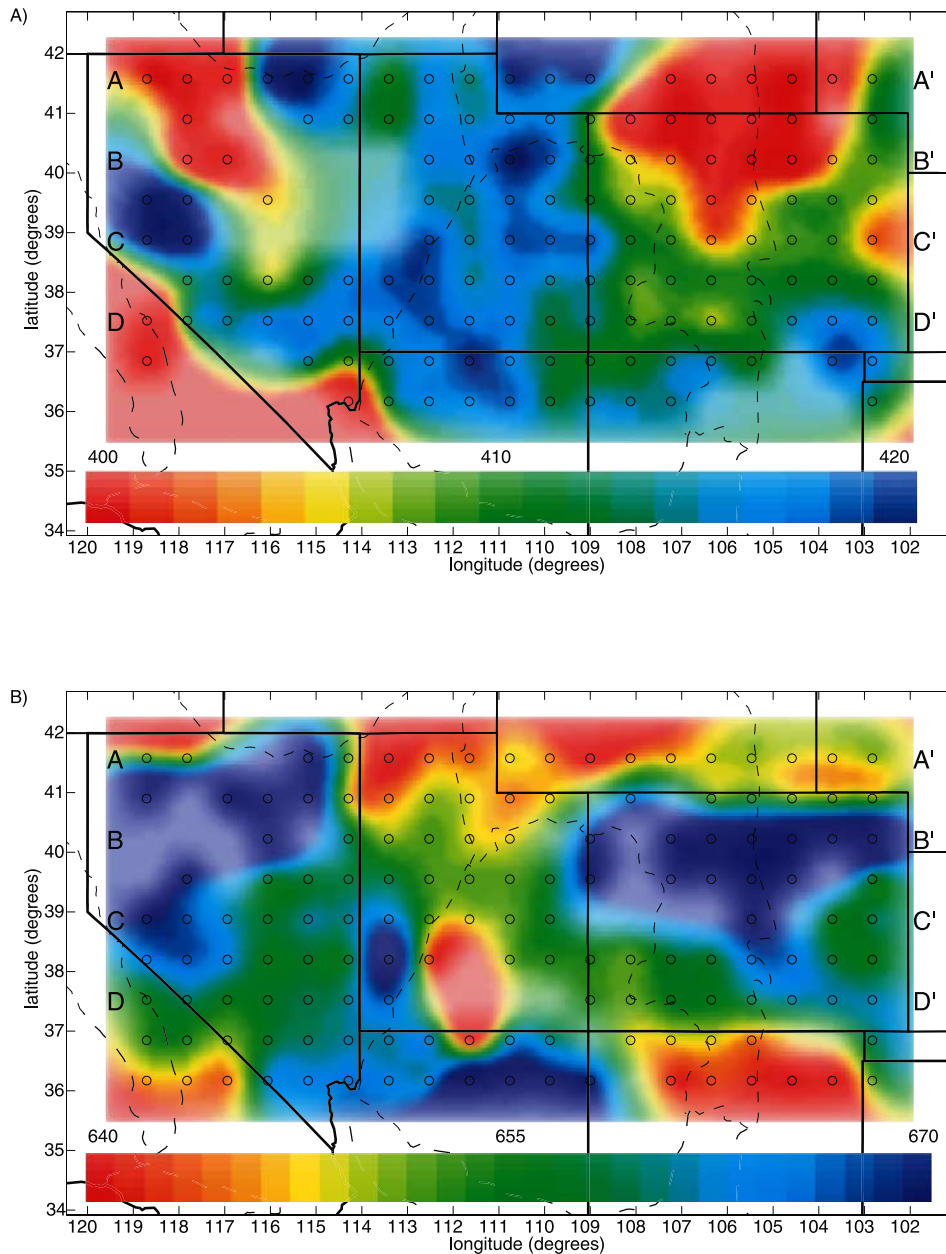
Figure 7. Same as Figure 6, except lateral heterogeneities in seismic wave speeds have been ignored.

piercing point stacks. For this test traces were randomly assigned to each bin and then processed in the manner described above. The geographic variations in resolution were maintained by using the same number of traces within each bin and the same lateral averaging and smoothing as above. If observed discontinuity topography were an artifact of noise or other aspects of the processing, similar lateral scales would be observed on both the randomized and properly binned discontinuity image. Instead, the randomized image shows almost no structure, for the 410- and 660-km discontinuities are essentially flat with depths varying by less than 3 km (Figure 11).

[17] In addition to depth variations, stacked amplitudes of $P_d s$ phases display variable amplitudes from as much as 15% of the radial P amplitude to less than 6% of it over distances as short as 225 km (Figures 12a–12d). In some regions the amplitudes of the pulse shapes appear diminished, while still possessing the same width. In other regions it appears that as the amplitudes of pulses diminish, their widths increase. The 410-km discontinuity arrival is weak below the middle of the Colorado Plateau (longitude 110°W in Figure 12a), as well as in the central and northern Basin and Range (from longitudes 117°W to 114°W part of Figures 12b and 12c). $P_{660}s$ phases are weak below northern Basin and Range (from longitudes 118°W to 113°W of Figure 12a) as well as below the central to northern Colorado Plateau (longitudes 112°W to 110°W of Figures 12b, 12c, and 12d). Some regions that are sampled by rays showing a strong $P_{660}s$ signal show a weak $P_{410}s$. Variations in the amplitude of the $P_d s$ phase do not depend on the number of traces or the back azimuth from which the traces come. By studying extensive regions of the

mantle lateral variations in discontinuity reflectivity become more apparent than when investigating only smaller regions.

[18] The pulse shapes of the $P_{660}s$ phase do not appear to be as symmetric as those of the $P_{410}s$ phase (Figures 12b and 12c). Instead, the onset of $P_{660}s$ appears sharp and decays gradually after it peaks. The asymmetric pulse shape could result from a gentler gradient in impedance below the discontinuity than above it. This asymmetric pulse is not always present, however, and in the western portion of the southern Basin and Range (longitude 117°W of Figure 12d), the $P_{660}s$ pulses appear symmetrical.

3.2. Other P_ds Arrivals

[19] In the depth range of 250 to 300 km, we observe another P_ds arrival (Figures 12a–12d and 13). This P_ds arrival is positively polarized, like those of $P_{410}s$ and $P_{660}s$ phases, which indicates a layer of higher shear wave impedance overlain by a layer of lower impedance. Numerous other studies have found evidence for P-to-S converted phases originating near this depth [see *Sheehan et al.*, 2000]. The base of a low-velocity zone, possibly due to partial melting, has been suggested for this discontinuity [*Lehmann*, 1959; *Vidale and Benz*, 1992]. Other proposed mechanisms include the transition from anisotropic lithosphere to isotropic mantle [*Gaherty and Jordan*, 1995] and the phase transition from coesite to stishovite [*Williams and Revenaugh*, 2000] that occur at pressures corresponding to this depth. Caution must be used, however, in interpreting arrivals observed within this time window because reverberations within the crust are also expected near this same time. Because arrivals converted at a depth of 250 km have smaller moveout than those from deeper phases, such as $P_{660}s$, testing whether or not the proposed $P_{250}s$ shows proper moveout, and determining the origin of this arrival, remain equivocal (Figure 13).

[20] We commonly observe an arrival between the $P_{410}s$ and $P_{660}s$ phases corresponding to a depth near 500 km (Figure 12). The wide range of depths and amplitudes of this arrival decreases the likelihood of it originating from a laterally continuous interface. The depth of this arrival does not appear correlated with the depths of either the 410- or the 660-km discontinuities. Amplitudes of the arrival from the suspected $P_{520}s$ phase are much smaller and broader than those of both the $P_{410}s$ and $P_{660}s$ phases. In some regions of the transition zone it appears that only one arrival between the 410 and 660 is present (e.g., longitude 113°W on Figure 12d), but in others instead of only a single, potential arrival from the 520-km discontinuity, multiple arrivals are present (e.g., longitude 105°W on Figure 12c).
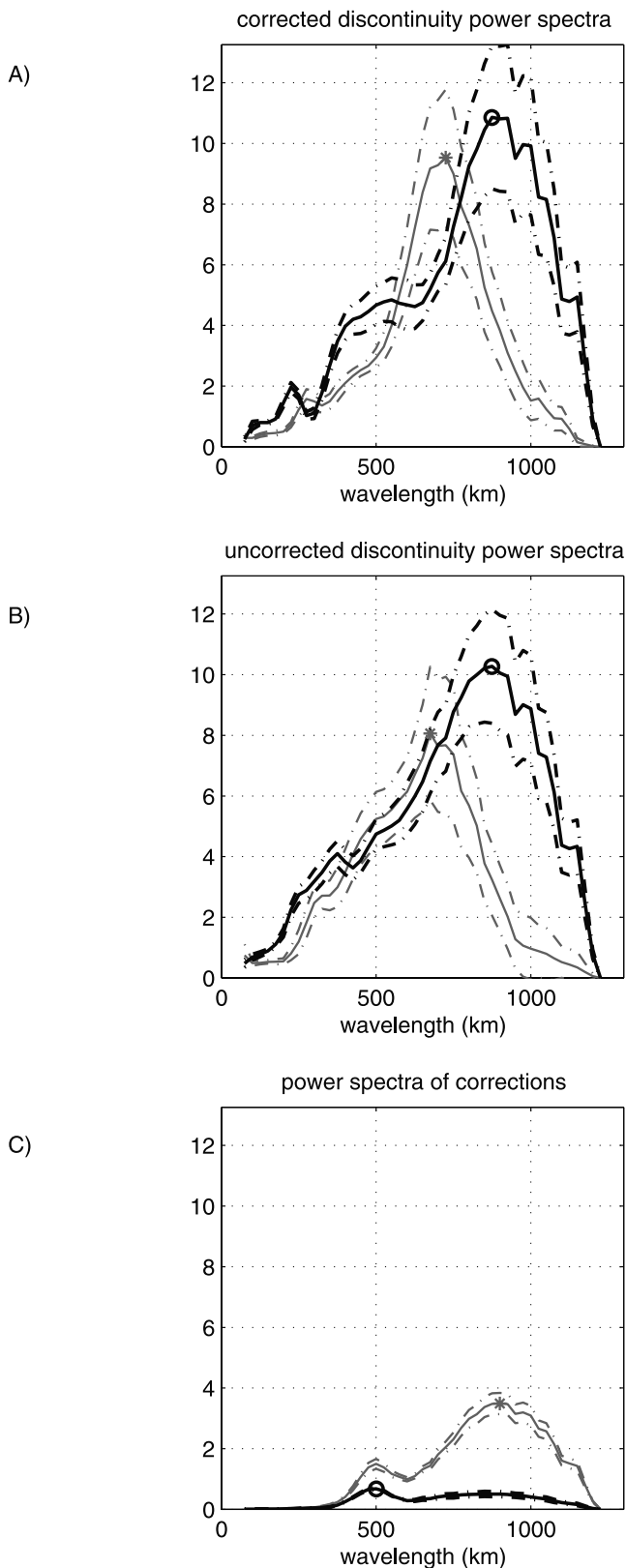
A)

corrected discontinuity power spectra

B)

uncorrected discontinuity power spectra

C)

power spectra of corrections

Figure 8. (opposite) (a) Two-dimensional power spectra illustrating the dominant wavelength of the two discontinuity surfaces with one standard deviation of spectra. Spectrum of the 410-km discontinuity is shown as solid, and spectrum of the 660-km discontinuity is shown as shaded. The peak of the 660-km discontinuity is at 725-km (asterisk) and the peak of the 410-km discontinuity is at 875 km (circle). Uncertainties in the discontinuity surfaces spectra have been calculated by finding the standard deviation of 100 bootstrap realizations of the discontinuities surfaces that lie within the error associated with each column of conversion point bins. (b) Same as Figure 8a, except made from discontinuity surfaces found when ignoring lateral heterogeneity in seismic wave speeds. (c) Same as Figure 8a expect made from applying timing corrections to flat surfaces.
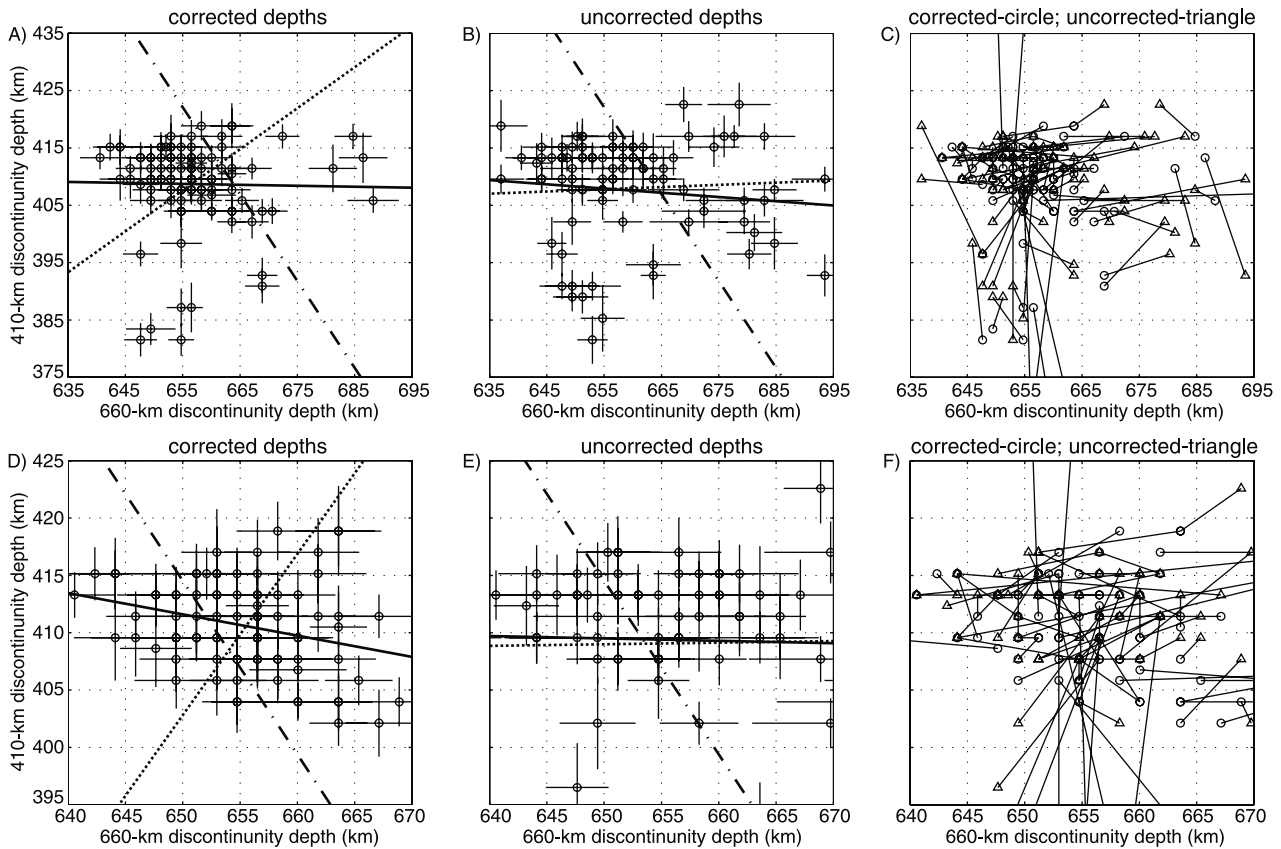
Figure 9. (a) The 410-km discontinuity depths versus 660-km discontinuity depths. Only data from columns in which well determined points with uncertainties less than 9 km for both discontinuities are plotted. These are the same points that are plotted as open circles in Figures 6 and 7. The least squares fit, calculated using *York*'s [1969] method of least squares fitting which accounts for errors in both data sets, between the two data sets (dotted line) illustrates the lack of any significant correlation. The fit found using standard least squares fitting, which ignores uncertainties is shown as a solid black line. The dashed line illustrates the relation predicted by the Clapeyron slopes of the two discontinuities (3.0 Mpa/K for the 410-km discontinuity and −2 Mpa/K for the 660-km discontinuity) affected by the same thermal perturbation. Error bars found using bootstrap resampling are shown for each point. (b) Same as Figure 9a, except no corrections for lateral heterogeneities were made in finding discontinuity depths. (c) Plot joining points from Figures 9a and 9b, corrected depths are plotted as circles, while uncorrected depths and plotted as triangles. Points from the same column of bins are joined. (d−f) Correspond to Figure 9a−9c, respectively, except that points with large deviations of corrected depths are not included.

Similar findings of a multipeaked arrival from the 520-km discontinuity have also been reported by global studies investigating characteristics of *SS* precursor arrivals [*Duess and Woodhouse*, 2001].

3.3. Influences on Discontinuity Imaging

[21] Factors independent of discontinuities can affect how they are imaged. Anisotropy shallower than 400 km can advance or delay travel times of both $P_{410}s$ and $P_{660}s$ phases depending on the azimuth of the $P_d s$ wave and orientation of anisotropic material. Little coherent shear wave splitting has been found on the northern Colorado Plateau, Rocky Mountains, and the central Basin and Range, but the transition between the Colorado Plateau and Basin and Range exhibits shear wave splitting of 1.0 s [*Savage and Sheehan*, 2000]. Anisotropic material that splits shear waves by 1.0 s could perturb arrival times of $P_d s$ phases an amount

that would correspond to 10 km of discontinuity topography. Combining data from different back azimuths from this region should average together azimuthal anisotropic effects but degrade the stacked data by introducing slight time shifts to arrivals that originated at the same depth. The majority of anisotropic material is thought to be at shallow depths above 200 km so that both the $P_{410}s$ and $P_{660}s$ phases would traverse the same amount of anisotropic material and would be affected in a similar manner. We do not observe collocated sharpness variations of the $P_{410}s$ and $P_{660}s$ phases suggesting that anisotropy does not contribute significantly to our observations.

[22] Amplitudes of $P_d s$ phases relate to the conversion coefficient of the interface where they were produced, which depends on the angle of incidence of the incoming wave. Thus an additional source of variation in stacked receiver functions could result from certain areas being
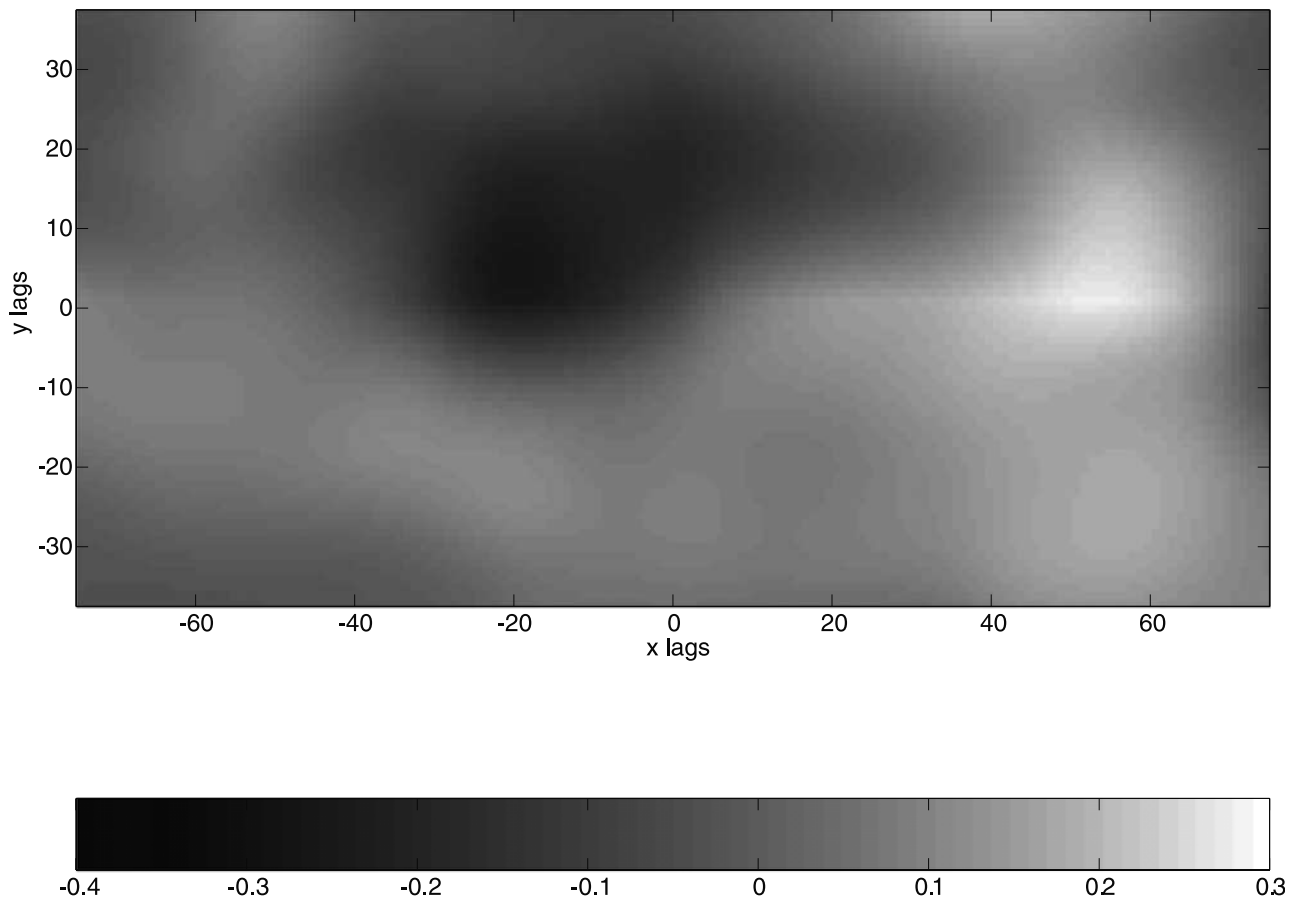
Figure 10. Two-dimensional cross correlation of 410- and 660-km discontinuity surfaces. Each lag in x and y directions corresponds to a 10-km shift in the interpolated 410-km discontinuity surface relative to the 660-km discontinuity. The range in correlation coefficients shown here is between a maximum value of 0.3 (light) and a minimum of −0.3 (dark). The correlation coefficient for the unshifted discontinuities with coordinates of 0 x lags and 0 y lags is 0.1.

sampled by events with a single angle of incidence. Most regions of the study area, however, are sampled by events from a similar range of diverse distances. The average amplitude of $P_d s$ waves with higher slownesses between 0.07 and 0.08 s/km, from a shallow incidence angle, is 6.3% the amplitude of radial P, but those of steeply incident $P_d s$ waves with lower slownesses between 0.04 and 0.05 s/km is 6.1%. Differences in amplitudes of converted phases from less than 5% to 15% of those of the P phase cannot be simply attributed to variations due to angle of incidence.

4. Discussion

[23] Other studies have suggested links between tectonic environments and transition zone structure. Signatures of warm material have been reported from thin transition zone thickness beneath Hawaii [*Li et al.*, 2000] and Iceland [*Shen et al.*, 1998b]. Near subduction zones, the discontinuities have been found to behave as affected by cold material with the 410-km discontinuity elevated to shallower depths and the 660-km discontinuity deepened [*Collier and Helffrich*, 1997, 2001; *Gilbert et al.*, 2001]. For such settings, the connections between surface tectonics and processes as deep as the transition zone have been established, whereas

in other settings, such relationships are less clear. Correlations have been identified between surface tectonics and seismic wave speeds at depths less than 200 km in parts of the western United States [*Humphreys and Dueker*, 1994]. We see no clear correlation between the different tectonic settings of the western United States and the upper mantle discontinuities at 410 km and 660 km depths. A similar lack of correlation between the upper mantle discontinuities and surface tectonics has been observed along the East Pacific Rise where the structures of neither the 410- nor 660-km discontinuities correlate with warm material in the uppermost mantle beneath the spreading center [*Shen et al.*, 1998a].

[24] Below the Rocky Mountains in northern Colorado the 410-km discontinuity shallows and the 660-km discontinuity deepens suggesting the presence of cold material in the transition zone that could relate to the development of the overlying mountain range. Studies have suggested that blobs of cold material below mountain ranges might detach and descend into the mantle causing mountain ranges to rise further isostatically [e.g., *Chen et al.*, 1997]. Perhaps a sinking piece of cold upper mantle is present here in the transition zone. Beneath the Rockies in southern Colorado, however, we do not observe similarly anti-correlated depths of discontinuities as if affected by sinking cold material.
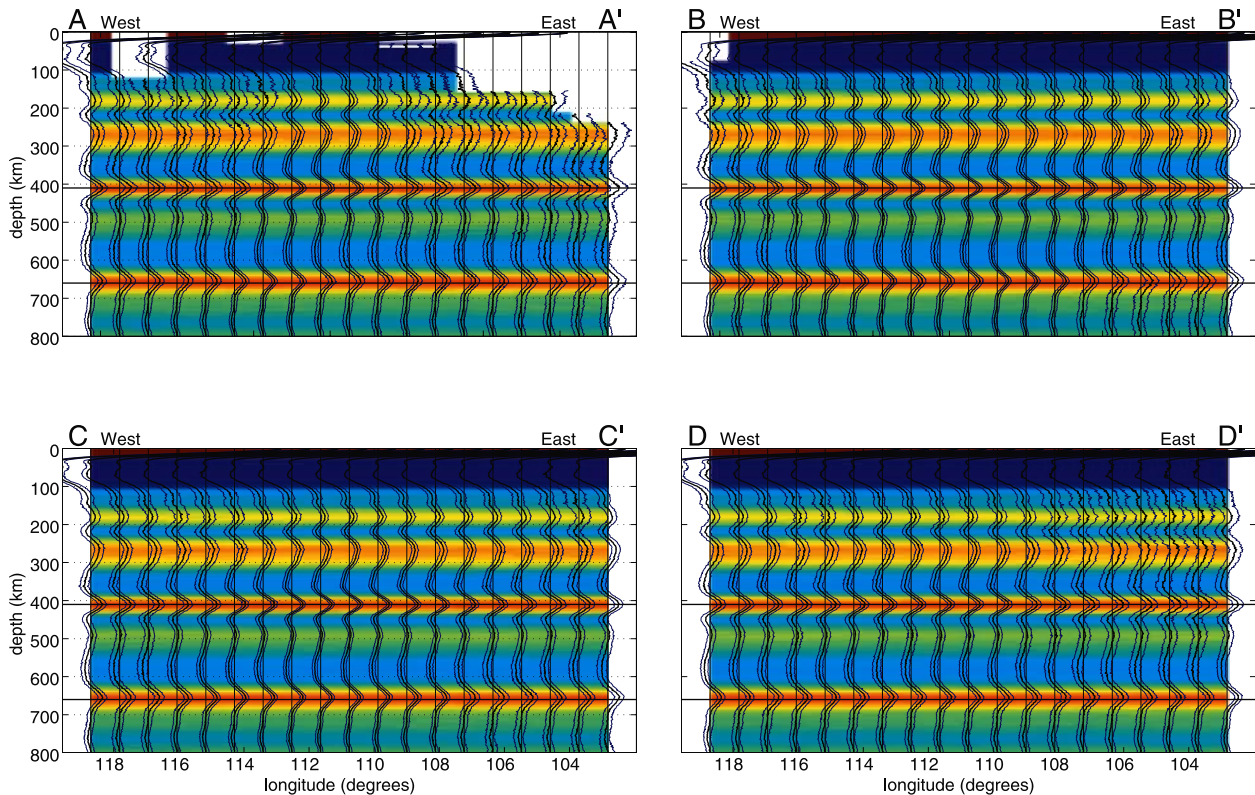
Figure 11. Randomized conversion point stacks. To test whether the observed discontinuity topography is some sort of artifact, we randomize the data geographically to observe if similar scale structure is present in geographically random data as in the correctly stacked data. Locations of cross-sections are shown on Figures 6 and 7. Common conversion point stacked receiver functions are plotted as bold black traces with one standard deviation, as determined from bootstraps, shown as blue traces. Color scale ranges between ±10% (positive, red, and negative, blue) of radial P.

Below most of the Colorado Plateau, the 410-km discontinuity is relatively deep, but the 660-km discontinuity deepens and shallows without correlation with the 410-km discontinuity. The 410-km discontinuity is deep below much of the Basin and Range, with exceptions in the northern and southern parts. The 660-km discontinuity is also deep below much of the Basin and Range but not in the southeastern portion where the discontinuity is close to its average depth. The lack of correlation in depths of the 410- and 660-km discontinuity provides no support for the idea that warm material at transition zone depths rises from a lower mantle source and passes through the transition zone to force up the high elevations and surface topography of the western United States. If processes originating in the transition zone or below it were responsible for, or even related to, the surface tectonics in the western United States, they must be subtle enough not to perturb the transition zone in a correlated manner. More likely the tectonic processes acting in the western United States have origins in the upper mantle shallower than the transition zone.

[25] On the basis of seismic tomography, *van der Lee and Nolet* [1997] proposed that remnants of the subducted Farallon plate linger in the upper mantle of this area. Clear evidence for the deflection of the mantle seismic discontinuities due to such a slab, however, are not detected, though compositional heterogeneities and fluids associated with a slab could contribute to the observed complex transition zone structure. We discuss possible mechanisms that could produce the observed discontinuity perturbations.

4.1. Thermal Variations

[26] Depths of the discontinuities are commonly used to ascertain thermal variations in the mantle. Variations in depths of discontinuities, however, can result from either thermal or compositional changes. If the only factors responsible for producing variations in discontinuity depths were thermal perturbations that shift the pressures at which the olivine to wadsleyite and ringwoodite to perovskite + magnesiowustite phase transitions occur, the same temperature anomaly at depths of 410 and 660 km should produce anti-correlated topography on the discontinuities. In numerous regions where known thermal anomalies exist in the transition zone, the discontinuity depths shift in a manner similar to that predicted by thermal effects modifying the pressures at which the phase transitions occur [e.g., *Collier and Helffrich*, 2001]. Evidence that transition zone thicknesses and seismic wave speed variations correlate below East Asia and Australia is also consistent with phase transitions of olivine and its higher-pressure polymorphs being responsible for the discontinuities [*Lebedev et al.*, 2002]. Therefore, in regions where mantle temperatures cannot be predicted, a sensible hypothesis for variations in depths of discontinuities is lateral differences in temperature.
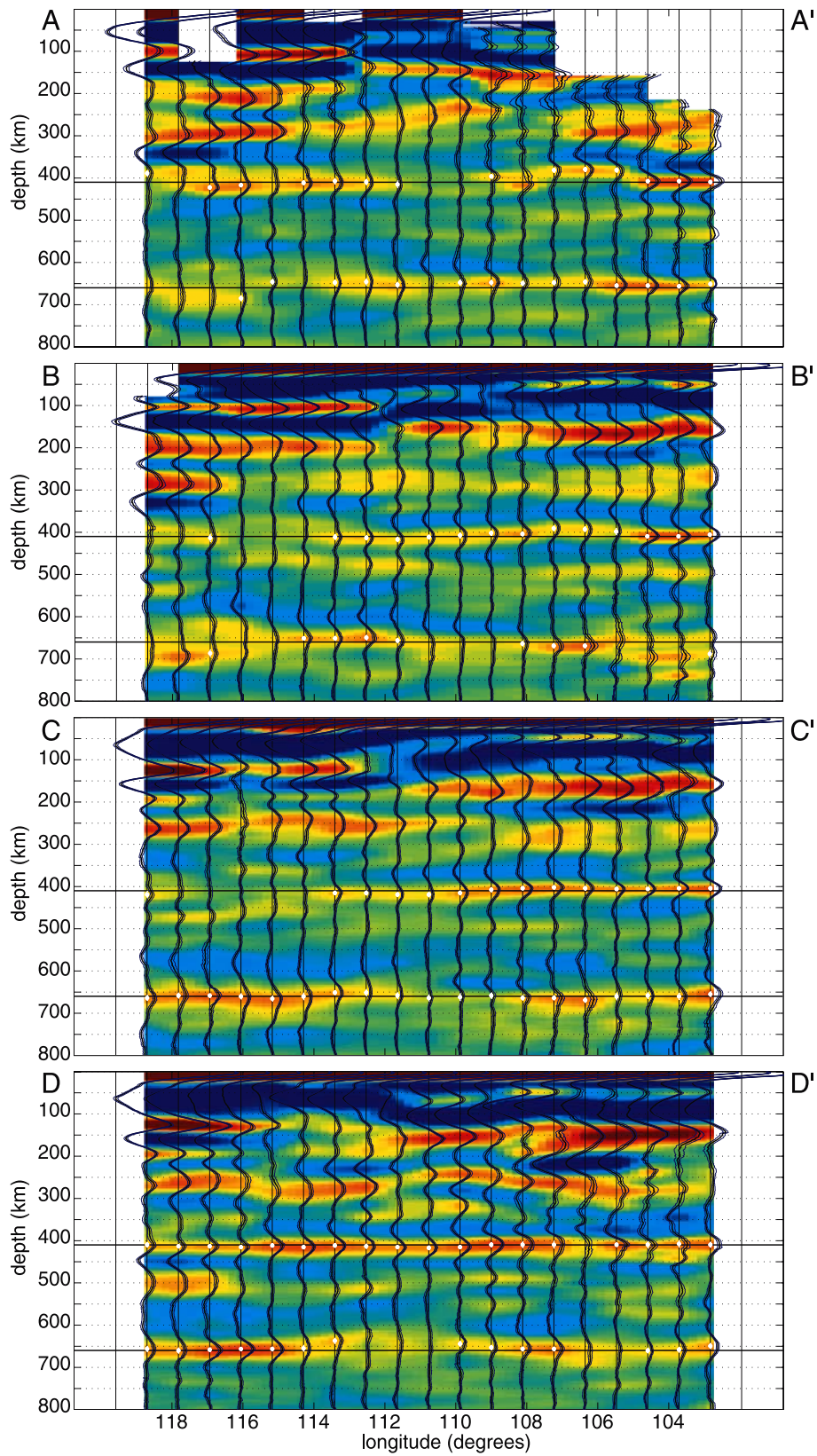
Figure 12. (a−d) West to east cross-sections of CCP stacked receiver functions. Locations of cross-sections are indicated on Figures 6 and 7 (A-A′, etc.). Radial *P* waves are scaled to unity for each trace. Color scale ranges between ±10% (positive, red, and negative, blue) of radial *P*. Stacked receiver functions are shown in black, and thinner blue lines are one sigma bounds derived from bootstrap resampling. White circles show picked depths found within each bin used to make discontinuity maps.
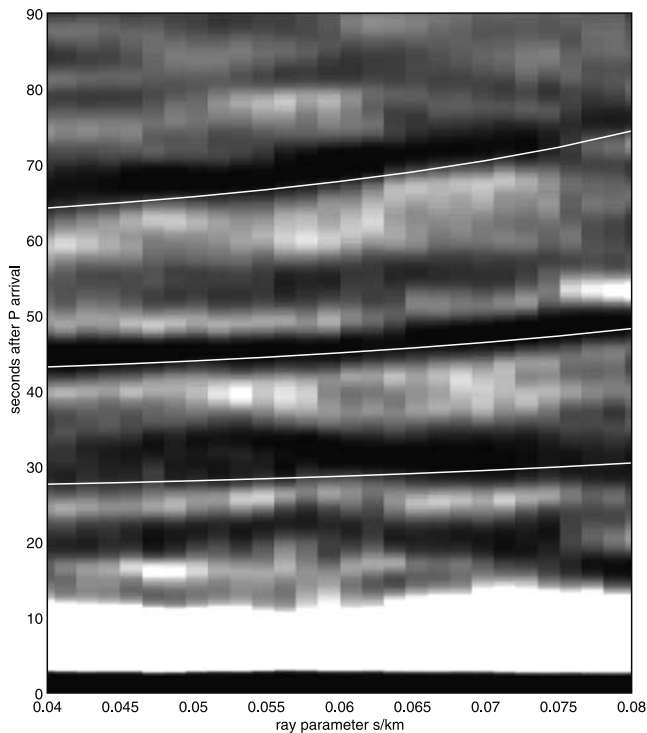
Figure 13. Radial receiver function phasing diagram. Each receiver function is binned with others with like slownesses and plotted as a function of slowness. Positive amplitudes are plotted darker, while negative are plotted lighter. Variations in arrival time of phases with increasing slowness can be easily seen for both the 410- and 660-km discontinuities. Theoretical arrival times predicted by TNA one-dimensional model are shown for discontinuities at 250, 410, and 660 km depths.

[27] The amount of topography observed here is comparable to that found near subduction zones [*Gilbert et al.*, 2001], suggesting the presence of comparable lateral thermal variations in the upper mantle. Unlike at subduction zones, however, the topography that we observe on the 410-km discontinuity does not correlate to the topography on the 660-km discontinuity even after accounting for possible offsets as demonstrated by the cross-correlation tests (Figure 10). Numerous other studies using both *SS* precursors, sensitive to variations over horizontal distances of 1000 km [*Flanagan and Shearer*, 1998; *Gu et al.*, 1998], and P_ds studies, sensitive to variations over distances of hundreds of kilometers [*Dueker and Sheehan*, 1997; *Li et al.*, 1998; *Owens et al.*, 2000; *Simmons and Gurrola*, 2000], have also found uncorrelated discontinuity topography. The results of *Li et al.* [1998] are particularly relevant to findings presented here as their study also presents observations of uncorrelated discontinuity structure over a region ~1500 km in length. Although that study did not sample a wide three-dimensional region, the wavelengths of discontinuity topography that they imaged along profiles below the eastern United States appear to be similar to that found here.

4.2. Possible Implications for Convective Structure

[28] A possible explanation for the uncorrelated discontinuity topography beneath the western United States is that thermal variations at 410 km depth are influenced by small-scale convective flow in the upper mantle, while convection in both the upper and lower mantle influences the depth of the 660-km discontinuity. The depths of the discontinuities need not be correlated if convective flow in the upper and lower mantle affects the depths of each discontinuity separately [e.g., *Busse*, 1981].

[29] Some combination of conditions might restrict flow from crossing between the upper and lower mantle, with chemical differences and a sufficiently negative Clapeyron slope in pressure-temperature space of the phase boundary at 660 km commonly cited as having strong influences [*Christensen and Yuen*, 1984; *Richter and McKenzie*, 1981]. Numerical experiments of *Christensen and Yuen* [1984] place quite narrow bounds on compositional and thermodynamic characteristics of the 660-km discontinuity that could cause convection to be layered; either composition differences with a density difference of 5% or a Clapeyron slope more negative than ~−6 MPa/K could prevent convective flow from penetrating this phase boundary. Early considerations of either possibility considered mineralogical phase changes of ringwoodite (γ-spinel) to perovskite + magnesiowustite at 660 km, for which the Clapeyron slope is ~−2 MPa/K [*Bina and Helffrich*, 1994]. Discussions of the density difference between the upper and lower mantle due to chemical differences have focused on the concentration of iron; by virtue of its large atomic weight, relatively small differences in its concentration between the upper and lower mantle might allow a sufficiently large density contrast across the transition zone to prevent convection [*Jeanloz and Knittle*, 1989]. Subsequent work, however, has cast doubt on the existence of a large compositional boundary and shows that models of seismic wave speeds require no compositional variation [*Wang et al.*, 1994]. Furthermore, the temperature profile between the inner and outer core that would result from the presence of a thermal boundary layer associated with compositional layering in the transition zone appears to be inconsistent with melting measurements of iron [*Chopelas and Boehler*, 1992]. Despite careful studies of Clapeyron slopes and chemical differences, a number of complexities continue to prevent definitive statements about the role of phase boundaries in mantle convection, such as multiple phase transitions, a coefficient of thermal expansion decreasing with depth [*Zhao et al.*, 1992], or viscosity stratification [*Kido and Yuen*, 2000]. Thus, despite thorough analysis by *Christensen and Yuen* [1984], there still seems to be enough uncertainty in the structure of the upper mantle to permit layered convection.

[30] Frequently, skeptics of layered convection rely on tomographic studies that reveal continuous high-wave speed anomalies in the lower mantle hypothesized to be subducted slabs now sinking through the lower mantle [*Grand*, 1994; *Grand et al.*, 1997; *van der Hilst et al.*, 1997]. However, models of seismic wave speeds with discontinuous features across the 660-km discontinuity have been found to fit observed travel time residuals as well as those with continuous features [*Gu et al.*, 2001]. Additionally, *Davaille's* [1999] experimental study of convection in two layered fluids showed that regions where cold material descends in the upper layer overlie similar flow in the lower layer and

thus renders the interpretation of global tomograms in terms of whole mantle convection nonunique.

[31] Suppose small-scale convection were confined to a layer 400–600 km in thickness, across which there was a superadiabatic temperature drop of 500°C. The corresponding Rayleigh number would be between 3×10^5 and 10^6. For Rayleigh numbers less than $\sim 10^5$, planforms of convection commonly develop with a characteristic wavelength roughly twice the thickness of the convecting layer [e.g., *Busse*, 1967, 1981; *Busse and Whitehead*, 1971, 1974; *Richter and Parsons*, 1975; *White*, 1988]. At higher Rayleigh numbers, where time-dependent detachment of boundary layers becomes important [e.g., *Howard*, 1966], the characteristic wavelength decreases gradually, but for Rayleigh numbers as large as 10^6, characteristic wavelengths are still approximately twice the layer thickness [e.g., *Whitehead and Parsons*, 1978; *Tackley*, 1996]. Thus, if convection were confined to the upper mantle, its planform should be characterized by a typical spacing between upwelling and downwelling regions of $\sim 800–1200$ km.

[32] Plots of the topography on both discontinuities (Figures 6 and 7) show a characteristic distance of ~ 800 km between highs or lows, as might be expected for small-scale convection confined to the upper mantle. Unfortunately, the dimensions of the region that we have studied do not allow a definitive statement of the characteristic wavelength, for the north-south dimension of the region studies is only 800 km. The east-west dimension of 1500 km, however, allows a two-dimensional spectrum to include longer wavelengths. Two-dimensional power spectra of both the 410- and the 660-km discontinuities exhibit distinct peaks at a wavelength near 800 km, with lower spectral densities at the fewer longer wavelengths that could be sampled (Figure 8). Thus the dominant wavelength differs little from what might be expected for layered convection and we determine that we do not find a spectral peak at a shorter wavelength.

4.3. Compositional Variations

[33] If the variations in the depths of the discontinuities observed here do not reflect thermal anomalies that may be associated with small-scale convection, some other factor must contribute to the observed discontinuity structure. Uncorrelated discontinuity topography might still exist in a mantle with a vertically coherent thermal structure if either or both of the discontinuities did not reflect thermally modulated depths of olivine phase transitions and its high-pressure polymorphs. Compositional heterogeneity can also contribute to discontinuity structure.

[34] The presence of hydrogen, structurally bound in mantle minerals, has been found both to broaden the olivine to wadsleyite phase loop and to cause it to occur at lower pressures [*Wood*, 1995]. Qualitatively, we do not observe a correlation between the depth of the 410-km discontinuity and the width of the $P_{410}s$ phase, which suggests that lateral variations in hydrogen content of the upper mantle do not cause the observed depth fluctuations of the 410-km discontinuity. Hydrogen may also affect the depth of the 660-km discontinuity as it has been found to be soluble in both ringwoodite [*Kohlstedt et al.*, 1996] and perovskite [*Meade et al.*, 1994].

[35] *Yusa and Inoue* [1997] have shown that juxtaposing dry olivine against wadsleyite including 1–2 wt% H_2O

reduces the amplitude of the impedance contrast across the 410-km discontinuity. Sharpness and amplitude variations observed here coincide both with lateral variations in structure and with regions where discontinuities appear planar. Additional complications in imaging discontinuity structure can result from non-planar interfaces causing focusing and defocusing of the $P_{d}s$ wave field [*van der Lee et al.*, 1994]. To avoid interpretation of results that may be contaminated by focusing and defocusing, we restrict our attention to pulse shape variations in regions with little topography. As variations in $P_{660}s$ pulse shapes commonly coincide with laterally varying depths of the 660-km discontinuity, we consider only $P_{410}s$ phases where the 410-km discontinuity is flat. Lateral variations in the hydrogen content within the mantle below the western United States could potentially produce the observed variations in the amplitude and sharpness of the 410-km discontinuity.

[36] *Stixrude* [1997] suggested an additional factor that could contribute to the sharpness of the 410-km discontinuity; the presence of non-transforming minerals together with the olivine component of the mantle, such as pyroxene and garnet, decrease the width of the olivine-waysleyite transition to half that of the binary phase loop. *Irifune and Isshiki* [1998] demonstrated that as olivine transforms to higher-pressure forms, the composition of the untransformed olivine changes due to chemical interaction between coexisting phases. In particular, the formation of majorite garnet at pressures between 10 and 15 GPa influences the olivine to wadsleyite transition by reducing its transition interval to from 0.6 GPa to 0.2 GPa (20 to 6 km), which is consistent with seismic observations [*Irifune and Isshiki*, 1998]. If lateral differences in the olivine composition exist in the transition zone, they may expand or contract this interval and alter the sharpness of the 410-km discontinuity.

[37] In the pyrolite model only $\sim 60\%$ of upper mantle mineralogy between 410 and 660 km depths consists of olivine polymorphs. Approximately 30% by volume consists of garnet, which not only can transform either directly to perovskite or first to ilmenite and then perovskite, but also does so with a large positive Clapeyron slope [*Weidner and Wang*, 1998]. *Weidner and Wang* [1998] argued that if garnet were devoid of aluminum, the large positive Clapeyron slopes for both garnet-perovskite and garnet ilmenite would overwhelm the negative slope for spinel-perovskite and make the combination of spinel and garnet negatively buoyant despite the negative Clapeyron slope for spinel-perovskite. The presence of aluminum, however, both broadens the depth range over which garnet transforms to perovskite and affects the fraction of olivine and pyroxene transforming to perovskite. The buoyancy of the assemblage thus depends on both the amount of aluminum and temperature.

[38] Studies examining phase equilibrium of minerals stable at 660 km, have found that at mantle temperatures of 1900K at the 660-km discontinuity, in the presence of other minerals, the amount of ringwoodite decreases with increasing pressure and the amount of garnet increases [e.g., *Weidner and Wang*, 1998]. The reduced amount of ringwoodite results in no observable ringwoodite to perovskite + magnesiowustite transition. Instead, a garnet-perovskite transition occurs at greater depth than that at which the ringwoodite transition should occur under similar mantle

temperatures, and produces a deep 660-km discontinuity [*Weidner and Wang*, 1998]. Thus depending upon the temperature and mineralogy of the mantle, a deep 660-km discontinuity could occur in either warm or cold regions of mantle. In contrast, *Wood* [2000] suggested that the garnet-pyroxene transition occurs over too broad a pressure range to produce an observable seismic discontinuity, but perhaps is responsible for high-velocity gradients below the 660-km discontinuity. Observations of higher-frequency (0.3Hz) $P_d s$ arrivals possibly resulting from a garnet phase transition have been reported in the region of southern California to the west of the region investigated here [*Simmons and Gurrola*, 2000]. We observe a slow decay after the peak of the $P_{660}s$ phase that could be attributed to high-velocity gradients resulting from the garnet-perovskite transition in the 660 to 760 km depth range.

[39] The larger Clapeyron slope of the olivine to wadsleyite phase transition, responsible for the 410-km discontinuity, implies that the same thermal anomaly would produce greater depth variations on the 410-km discontinuity than on the 660-km discontinuity. In contrast, like most studies [e.g., *Flanagan and Shearer*, 1998; *Li et al.*, 1998], we find that the 660-km discontinuity exhibits greater amounts of topography than the 410-km discontinuity. Complications associated with how the discontinuities are imaged by studies using longer period phases have been suggested as a possible mechanism that could mask the additional topography of the 410-km discontinuity [*Helffrich*, 2000].

[40] Although compositional effects have the potential to contribute to discontinuity topography, recent studies [*Collier and Helffrich*, 2001; *Lebedev et al.*, 2002] have found that the discontinuities behave similarly to predictions based on thermally controlled phase transitions. Investigating the discontinuity depths near beneath South America, *Collier and Helffrich* [2001] find that the depth of the 410-km discontinuity compares favorably to discontinuity depths appropriate for a conductively warming slab subducted beneath South America and a Clapeyron slope of 2.04 MPa/K. While compositional heterogeneity associated with a subducted slab may be present in both South America and the western United States, a simple model based on thermal effects is adequate to explain the depths of the discontinuities below South America and therefore should be considered as a plausible cause of discontinuity topography in the western United States. The observations presented here show lateral variations in the reflectivity of the 410-km discontinuity, but no clear correlation between discontinuity depths and $P_{410}s$ amplitudes. Lateral variations in the Fe/Mg ratio of olivine could affect the sharpness of the 410-km discontinuity without affecting its depth as described by *Irifune and Isshiki* [1998]. A correlation between discontinuity sharpness and depth would be expected if variations in hydration were the only factor responsible for causing a decrease in discontinuity sharpness. Still, the variable presence of hydrogen also contributing to discontinuity structure cannot be ruled out.

5. Conclusions

[41] By combining data from multiple seismic arrays we image a large portion of upper mantle below the western United States. This study began with the goal of relating transition zone structure to dynamic stresses applied to the base of the lithosphere that might have created the diverse surface tectonics in the western United States, but little evidence was found for a connection between discontinuity structure and surface tectonics. Moreover, both the 410- and 660-km discontinuities exhibit 20 and 30 km of topography that is uncorrelated between the two. Other studies using similar methods have found comparable amounts of discontinuity topography [*Dueker and Sheehan*, 1997; *Shen et al.*, 1998b; *Li et al.*, 2000; *Owens et al.*, 2000], but these other investigations studied smaller regions and found some connection between upper mantle structure and regional tectonics.

[42] The sharpness of the upper mantle discontinuities varies across the study area, in some areas appearing narrow, but in others appearing broader and more diffuse. Observed fluctuations in the impedance contrast at the discontinuities may result from compositional influences on the discontinuity structure. Shifts in discontinuity depths that do not correspond to sharpness variations are consistent with variations in the Fe/Mg ratio of olivine influencing the sharpness of the 410-km discontinuity, but alterations in the hydration state or in the proportion of olivine to coexisting minerals in the mantle could also affect the discontinuity sharpness. Details of the extent to which compositional variations modify discontinuity depths are still not known, moreover, uncertainty exists as to mantle composition at transition zone depths. Better constraints on compositional influences will provide guidelines to determine how much discontinuity structure does not result from thermal influences, but compositional factors.

[43] If upper mantle discontinuity depths reflected thermal variations, the lack of correlation in the topography of the upper mantle discontinuities indicates that, at the scales imaged here, lateral variations in temperature at 410 km depth differ from those at 660 km. The absence of correlated discontinuity depths rules out rising and sinking plumes or sheets passing vertically though the transition zone beneath this region. The correlation is not significantly improved by applying lateral shifts, as might be expected from a dipping slab. A vertically incoherent thermal structure that could result from small-scale convection in the upper mantle could affect the 410 and 660 km discontinuities differently. Unless compositional heterogeneity in the upper mantle is responsible for the lateral variations in discontinuity depths that we report, small-scale convection offers a credible explanation for these variations.

References

Agee, C. B., Phase transformation and seismic structure in the upper mantle and the transition zone, in *Ultrahigh-Pressure Mineralogy: Physics and Chemistry of the Earth's Deep Interior*, *Rev. Mineral.*, vol. 37, edited by R. J. Hemley and H. K. Mao, pp. 165–203, Mineral. Soc. of Am., Washington, D. C., 1998.

Alsina, D., R. L. Woodward, and R. K. Snieder, Shear wave velocity structure in North America from large-scale waveform inversions of surface waves, *J. Geophys. Res.*, *101*, 15,969–15,986, 1996.

Bijwaard, H., W. Spakman, and E. R. Engdahl, Closing the gap between regional and global travel time tomography, *J. Geophys. Res.*, *103*, 30,055–30,078, 1998.

Bina, C. R., and G. Helffrich, Phase transition Clapeyron slopes and transition zone seismic discontinuity topography, *J. Geophys. Res.*, *99*, 15,853–15,860, 1994.

Bird, P., Continental delamination and the Colorado Plateau, *J. Geophys. Res.*, *84*, 7561–7571, 1979.

Bump, H., K. Dueker, A. F. Sheehan, C. H. Jones, A. Levander, D. McNamara, R. Palmer, G. Biasi, and G. Humphreys, Colorado Plateau crust and upper mantle structure from the Deep Probe Natural Source Experiment, *Eos Trans. AGU*, *76*(46), Fall Meet. Suppl., F604, 1995.

Busse, F. H., On the stability of two-dimensional convection in a layer heated from below, *J. Math Phys.*, *46*, 140–150, 1967.

Busse, F. H., On the aspect ratio of two-layer mantle convection, *Phys. Earth Planet. Inter.*, *24*, 320–324, 1981.

Busse, F. H., and J. Whitehead, Instabilities of convection rolls in a high Prandtl number fluid, *J. Fluid Mech.*, *47*, 305–320, 1971.

Busse, F. H., and J. A. Whitehead, Oscillatory and collective instabilities in large Prandtl number convection, *J. Fluid Mech.*, *66*, 67–79, 1974.

Chen, Y. H., S. W. Roecker, and G. L. Kosarev, Elevation of the 410 km discontinuity beneath the central Tein Shan: Evidence for a detached lithospheric root, *Geophys. Res. Lett.*, *24*, 1531–1534, 1997.

Chevrot, S., L. Vinnik, and J. P. Montagner, Global-scale analysis of the mantle Pds phases, *J. Geophys. Res.*, *104*, 20,203–20,219, 1999.

Chopelas, A., and R. Boehler, Thermal expansivity in the lower mantle, *Geophys. Res. Lett.*, *19*, 1983–1986, 1992.

Christensen, U. R., and D. A. Yuen, The interaction of a subducting lithospheric slab with a chemical or phase boundary, *J. Geophys. Res.*, *89*, 4389–4402, 1984.

Clouser, R. H., and C. A. Langston, Effect of sinusoidal interfaces on teleseismic *P*-wave receiver functions, *Geophys. J. Int.*, *123*, 541–558, 1995.

Collier, J. D., and G. R. Helffrich, Topography of the "410" and "660" km seismic discontinuities in the Izu-Bonin subduction zone, *Geophys. Res. Lett.*, *24*, 1535–1538, 1997.

Collier, J. D., and G. R. Helffrich, The thermal influence of the subducting slab beneath South America from 410 and 660 km discontinuity observations, *Geophys. J. Int.*, *147*, 319–329, 2001.

Davaille, A., Two-layer thermal convection in miscible viscous fluids, *J. Fluid Mech.*, *379*, 223–253, 1999.

Dueker, K. G., and E. Humphreys, Relationships between upper mantle velocity structure and the tectonic parabola along the Yellowstone volcanic trend, *Eos Trans. AGU*, *74*(43), Fall Meet. Suppl., F602, 1993.

Dueker, K. G., and A. F. Sheehan, Mantle discontinuity structure from midpoint stacks of converted *P* to *S* waves across the Yellowstone hotspot track, *J. Geophys. Res.*, *102*, 8313–8327, 1997.

Dueker, K. G., and A. F. Sheehan, Mantle discontinuity structure beneath the Colorado Rocky Mountains and High Plains, *J. Geophys. Res.*, *103*, 7153–7169, 1998.

Dueker, K., H. Yuan, and B. Zurek, Thick-structured Proterozoic lithosphere of the Rocky Mountain region, *GSA Today*, *11*, 4–9, 2001.

Duess, A., and J. Woodhouse, Seismic observations of splitting of the mid-transition zone discontinuity in the Earth's mantle, *Science*, *294*, 354–357, 2001.

Eaton, G. P., A tectonic redefinition of the southern Rocky Mountains, *Tectonophysics*, *132*, 163–193, 1986.

Efron, B., and R. Tibshirani, Bootstrap methods for standard errors, confidence intervals, and other measures of statistical accuracy, *Stat. Sci.*, *1*, 54–77, 1986.

Flanagan, M. P., and P. M. Shearer, Global mapping of topography on transition zone velocity discontinuities by stacking *SS* precursors, *J. Geophys. Res.*, *103*, 2673–2692, 1998.

Gaherty, J. B., and T. H. Jordan, Lehamann discontinuity as the base of an anisotropic layer beneath continents, *Science*, *268*, 1468–1471, 1995.

Gilbert, H. J., A. F. Sheehan, D. A. Weins, K. Dueker, L. Dorman, J. Hildebrand, and S. Webb, Upper mantle discontinuity structure in the region of the Tonga Subduction Zone, *Geophys. Res. Lett.*, *28*, 1855–1858, 2001.

Grand, S. P., Mantle shear structure beneath the Americas and surrounding oceans, *J. Geophys. Res.*, *99*, 11,591–11,621, 1994.

Grand, S. P., and D. V. Helmberger, Upper mantle shear structure of North-America, *Geophys. J. R. Astron. Soc.*, *76*, 399–438, 1984.

Grand, S. P., R. D. van der Hilst, and S. Widiyantoro, Global seismic tomography: A snapshot of convection in the Earth, *GSA Today*, *7*, 1–7, 1997.

Gu, Y., A. M. Dziewonski, and C. B. Agee, Global de-correlation of the topography of transition zone discontinuities, *Earth Planet. Sci. Lett.*, *157*, 57–67, 1998.

Gu, Y., A. M. Dziewonski, W. Su, and G. Ekstrom, Models of the mantle shear velocity and discontinuities in the pattern of lateral heterogeneities, *J. Geophys. Res.*, *106*, 11,169–11,199, 2001.

Helffrich, G., Topography of the transition zone seismic discontinuities, *Rev. Geophys.*, *38*, 141–158, 2000.

Humphreys, E. D., and K. G. Dueker, Western U.S. upper mantle structure, *J. Geophys. Res.*, *99*, 9615–9634, 1994.

Irifune, T., and M. Isshiki, Iron partitioning in a pyrolite mantle and the nature of the 410-km seismic discontinuity, *Nature*, *392*, 702–705, 1998.

Jeanloz, R., and E. Knittle, Density and composition of the lower mantle, *Philos. Trans. R. Soc. London, Ser. A*, *328*, 377–389, 1989.

Kido, M., and D. A. Yuen, The role played by a low viscosity zone under a 660 km discontinuity in regional mantle layering, *Earth Planet. Sci. Lett.*, *181*, 573–583, 2000.

Kohlstedt, D. L., H. Keppler, and D. C. Rubie, Solubility of water in the α, β and γ phases of $(Mg, Fe)_2SiO4$, *Contrib. Mineral. Petrol.*, *123*, 345–357, 1996.

Langston, C. A., Corvallis, Oregon, crustal and upper mantle receiver structure from teleseismic *P*-waves and *S*-waves, *Bull. Seismol. Soc. Am.*, *67*, 713–724, 1977.

Lebedev, S., S. Chevrot, and R. van der Hilst, Seismic evidence for olivine phase changes at the 410- and 660-kilometer discontinuities, *Science*, *296*, 1300–1302, 2002.

Lee, D. K., and S. P. Grand, Depth of the upper mantle discontinuities beneath the East Pacific Rise, *Geophys. Res. Lett.*, *23*, 3369–3372, 1996.

Lehmann, I., Velocities of longitudinal waves in the upper part of the Earth's mantle, *Ann. Geophys.*, *15*, 93–118, 1959.

Li, A. B., K. M. Fischer, M. E. Wysession, and T. J. Clarke, Mantle discontinuities and temperature under the North American continental keel, *Nature*, *395*, 160–163, 1998.

Li, X., S. V. Sobolev, R. Kind, X. Yuan, and C. Estabrook, A detailed receiver function image of the upper mantle discontinuities in the Japan subduction zone, *Earth Planet. Sci. Lett.*, *183*, 527–541, 2000.

McKenzie, D., Surface deformation, gravity anomalies and convection, *Geophys. J. R. Astron. Soc.*, *48*, 211–238, 1977.

Meade, C., J. A. Reffner, and E. Ito, Synchrotron infrared absorbance measurements of hydrogen in $MgSiO_3$ perovskite, *Science*, *264*, 1558–1560, 1994.

Owens, T. J., A. A. Nyblade, H. Gurrola, and C. A. Langston, Mantle transition zone structure beneath Tanzania, East Africa, *Geophys. Res. Lett.*, *27*, 827–830, 2000.

Parsons, B., and S. Daly, The relationship between surface topography, gravity anomalies, and temperature structure of convection, *J. Geophys. Res.*, *88*, 1129–1144, 1983.

Ramesh, D. S., R. Kind, and X. Yuan, Receiver function analysis of the North American crust and upper mantle, *Geophys. J. Int.*, *150*, 91–108, 2002.

Richards, M. A., and B. H. Hager, Geoid anomalies in a dynamic mantle, *J. Geophys. Res.*, *89*, 5987–6002, 1984.

Richter, F. M., and D. P. McKenzie, On some consequences and possible causes of layered mantle convection, *J. Geophys. Res.*, *86*, 6133–6142, 1981.

Richter, F. M., and B. Parsons, On the interaction of two scales of convection in the mantle, *J. Geophys. Res.*, *80*, 2529–2541, 1975.

Sandwell, D. T., Biharmonic spline interpolation of GEOS-3 and SEASAT altimeter data, *Geophys. Res. Lett.*, *14*, 139–142, 1987.

Savage, M. K., and A. F. Sheehan, Seismic anisotropy and mantle flow from the Great Basin to the Great Plains, western United States, *J. Geophys. Res.*, *105*, 13,715–13,734, 2000.

Sheehan, A. F., G. A. Abers, C. H. Jones, and L. A. L. Lerner, Crustal thickness variations across the Colorado Rocky Mountains from teleseismic receiver functions, *J. Geophys. Res.*, *100*, 20,391–20,404, 1995.

Sheehan, A. F., C. H. Jones, M. K. Savage, S. Ozalaybey, and J. M. Schneider, Contrasting lithospheric structure between the Colorado Plateau and Great Basin: Initial results from Colorado Plateau-Great Basin PASSCAL experiment, *Geophys. Res. Lett.*, *24*, 2609–2612, 1997.

Sheehan, A. F., P. M. Shearer, H. J. Gilbert, and K. G. Dueker, Seismic migration processing of *P-SV* converted phases for mantle discontinuity structure beneath the Snake River Plain, western United States, *J. Geophys. Res.*, *105*, 19,055–19,065, 2000.

Shen, Y., A. F. Sheehan, K. G. Dueker, C. de Groot-Hedlin, and H. Gilbert, Mantle discontinuity structure beneath the southern East Pacific Rise from *P*-to-*S* converted phases, *Science*, *280*, 1232–1235, 1998a.

Shen, Y., S. C. Solomon, I. T. Bjarnason, and C. J. Wolfe, Seismic evidence for a lower-mantle origin of the Iceland plume, *Nature*, *395*, 62–65, 1998b.

Simmons, N. A., and H. Gurrola, Multiple seismic discontinuities near the base of the transition zone in the Earth's mantle, *Nature*, *405*, 559–562, 2000.

Stixrude, L., Structure and sharpness of phase transitions and mantle discontinuities, *J. Geophys. Res.*, *102*, 14,835–14,52, 1997.

Tackley, P. J., On the ability of phase transitions and viscosity layering to induce long wavelength heterogeneity in the mantle, *Geophys. Res. Lett.*, *23*, 1985–1988, 1996.

van der Hilst, R. D., S. Widiyantoro, and E. R. Engdahl, Evidence for deep mantle circulation from global tomography, *Nature*, *386*, 578–584, 1997.

van der Lee, S., and G. Nolet, Upper mantle *S* velocity structure of North America, *J. Geophys. Res.*, *102*, 22,815–22,838, 1997.

van der Lee, S., H. Paulssen, and G. Nolet, Variability of *P660s* phases as a consequence of topography of the 660 km discontinuity, *Phys. Earth Planet. Inter.*, *86*, 147–164, 1994.

Vidale, J. E., and H. M. Benz, Upper-mantle seismic discontinuities and the thermal structure of subduction zones, *Nature*, *356*, 678–683, 1992.

Wang, Y., D. J. Weidner, R. C. Liebermann, and Y. Zhao, P-V-T equation of state of (Mg, Fe)SiO$_3$ perovskite: Constraints on composition of the lower mantle, *Phys. Earth Planet. Inter.*, *83*, 13–40, 1994.

Weidner, D. J., and Y. Wang, Chemical- and Clapeyron-induced buoyancy at the 660 km discontinuity, *J. Geophys. Res.*, *103*, 7431–7441, 1998.

White, D. B., The planforms and onset of concection with a temperature-dependent viscosity, *J. Fluid Mech.*, *191*, 247–286, 1988.

Whitehead, J. A., Jr., and B. Parsons, Observations of convection at Rayleigh numbers up to 760,000 in a fluid with large Prandtl number, Fluid models of geological hotspots, *Geophys. Astrophys. Fluid Dyn.*, *9*, 201–217, 1978.

Williams, Q., and J. Revenaugh, The X-discontinuity: A signature of deep fluid flow and free silica in the sub-continental mantle, *Eos Trans. AGU*, *81*(48), Abstract S21E-07, 2000.

Wood, B. J., The effect of H$_2$O on the 410-kilometer seismic discontinuity, *Science*, *286*, 74–76, 1995.

Wood, B. J., Phase transformations and partitioning relations in peridotite under lower mantle conditions, *Earth Planet. Sci. Lett.*, *174*, 341–354, 2000.

York, D., Least squares fitting of a straight line with correlated errors, *Earth Planet. Sci. Lett.*, *5*, 320–324, 1969.

Yusa, H., and T. Inoue, Compressibility of hydrous wadsleyite (β-phase) in Mg$_2$SiO$_4$ by high-pressure X ray diffraction, *Geophys. Res. Lett.*, *24*, 1831–1834, 1997.

Yusa, H., T. Inoue, and Y. Ohishi, Isothermal compressibility of hydrous ringwoodite and its relation to the mantle discontinuities, *Geophys. Res. Lett.*, *27*, 413–416, 2000.

Zhao, W., D. A. Yuen, and S. Honda, Multiple phase transitions and the style of mantle convection, *Phys. Earth Planet. Inter.*, *72*, 185–210, 1992.

_____

K. G. Dueker, Department of Geology and Geophysics, University of Wyoming, P.O. Box 3006, Laramie, WY 82071-3006, USA. (dueker@uwyo.edu)

H. J. Gilbert, Department of Geosciences, University of Arizona, 1040 E. 4th Street, Tucson, AZ 85721, USA. (hgilbert@geo.arizona.edu)

P. Molnar and A. F. Sheehan, Department of Geological Sciences, University of Colorado, Campus Box 399, Boulder, CO 80309-0399, USA. (molnar@cires.colorado.edu; afs@cires.colorado.edu)